CHARACTERIZATION AND QUANTIFICATION OF GROUND HEAT FLUX FOR LATE SEASON SHALLOW SNOW

by

Aurele LaMontagne

A thesis

Submitted in partial fulfillment

of the requirements for the degree of

Master of Science in Hydrologic Sciences

Boise State University

Summer, 2009

BOISE STATE UNIVERSITY GRADUATE COLLEGE

DEFENSE COMMITTEE AND FINAL READING APPROVALS

of the dissertation submitted by

Aurele LaMontagne

Dissertation Title: Characterization and Quantification of Ground Heat Flux for Late Season Shallow Snow

Date of Final Oral Examination: 03 April 2009

The following individuals read and discussed the dissertation submitted by student Stephanie Stacey Starr, and they also evaluated her presentation and response to questions during the final oral examination. They found that the student passed the final oral examination, and that the dissertation was satisfactory for a doctoral degree and ready for any final modifications that they explicitly required.

James P. McNamara, Ph.D. Chair, Supervisory Committee

Charles H. Luce, Ph.D. Member, Supervisory Committee

John H. Bradford, Ph.D. Member, Supervisory Committee

The final reading approval of the dissertation was granted by James P. McNamara, Ph.D., Chair of the Supervisory Committee. The dissertation was approved for the Graduate College by John R. Pelton, Ph.D., Dean of the Graduate College.

ACKNOWLEDGEMENTS

I would like to thank my family, advisor and committee members, remote assistants, fellow graduate students, and funding agencies for their contributions to this research. Thank you Paige, Tavish, and Owen, for your incredible patience and support throughout this effort. I thank my parents Armand and Virginia Lamontagne for encouraging their children to look beyond the horizon and pursue their dreams. I thank my advisor Dr. James P. McNamara for giving me this opportunity and providing many interesting research challenges. I am grateful for the critical technical assistance provided by my committee members Dr. Charles Luce and Dr. John Bradford, Dr. John Selker, Dr. Scott Tyler, and Mike Collier. Absolutely vital to this research was the technical assistance from John Dorighi, Agilant DTS engineer. Countless hours of field assistance was provided by Pam Ashlin, Mike Whitson, Ben Stratton, Mike Thoma, Matt Weaver, Ivan Geroy, Brian Anderson, and Daniella Makram-Morgos, and many others. The necessary funding was provided by NSF-Idaho EPSCoR Program and the National Science Foundation under award number EPS-0447689, the Boise State University Geoscience Department, and a Geological Society of America Graduate Research Grant. My final thanks go to my office mates known as the "Bulls" who provided so much comic relief and fishing opportunity it is a wonder any of us made it through the program.

ABSTRACT

Increasing populations, rapid land use changes, and climate change in mountainous areas have stressed water resources and reduced available water from snowpacks. In anticipation of warmer temperatures, receding snowlines, and increasing water demands, water managers will need detailed snowmelt energy and water balance information from the margin as transitional snow replaces deeper snowpacks. Patchy shallow snow, found at transitional snow elevations, has a distinct energy balance that includes local advection and short wave radiation penetration of snow less than 10 cm deep. Solar penetration to the soil surface provides a heat source that can be absorbed by the soil and conducted back to the snow. The objective of this study is to compare ground heat flux beneath snow less than 10 cm depth (shallow) and greater than 10 cm depth to see if solar penetration of shallow snow results in the heating of soils and an increased ground heat flux. Further objectives of the study are to evaluate the mathematical model for ground heat flux and to assess distributed temperature sensing (DTS) as a tool for measuring soil/snow interface temperatures beneath spatially unpredictable shallow snow extents.

To capture and quantify the additional energy flux below patches of spatially unpredictable shallow snow, near surface soil temperatures must be taken at large spatial scales. High spatial resolution DTS was deployed prior to snow season, 2.5 cm beneath the soil surface throughout a mid-elevation semi-arid watershed, to capture near surface soil temperatures below spatially unpredictable patchy snow. Ground heat flux was modeled from the soil temperatures.

The soil column in this study showed an increasing modeled ground heat flux as soil temperature measurement moved closer to the soil-snow interface. This trend violates the steady state assumption of the model with respect to the soil column and reveals that soil temperature measurement depth has a substantial inverse relationship with the magnitude of modeled ground heat flux

The DTS was successful in capturing soil temperatures beneath the unpredictable snow patches. However, due to DTS spatial averaging along the cable to produce point measurements, temperature accuracy was compromised. Despite the possible accuracy of ±0.04°C, this compromise lead to uncertainties in heat sources responsible for soil temperature differences beneath shallow and deep snow.

TABLE OF CONTENTS

LIST OF TABLES

LIST OF FIGURES

1. INTRODUCTION

One sixth of the world's population (Barnett et al. 2005) and sixty million people in the western United States are dependent on seasonal snowpacks for their water needs (Bales et al. 2006). Increasing populations and rapid land use changes in mountainous areas have stressed water resources while anthropogenic climate changes have reduced available water from snowpacks (Mote et al. 2005). Warmer temperatures have reduced snowpacks and caused earlier onsets of spring snowmelt (Cayan et al. 2001; Barnett et al. 2005; Stewart et al. 2005). In mountain areas of the western U.S., substantial portions of the annual precipitation fall at lower elevations having average winter temperatures of -3° to 0°C (Maurer et al. 2002 in Bales et al. 2006). As a result of current warming, and with possible increases of 3°C within the next hundred years, greater amounts of precipitation will fall as rain, spring runoff will occur earlier, flooding were more frequent, and available runoff and water storage for peak summer use will be reduced (Bales et al. 2006). In anticipation of warmer temperatures, receding snowlines, and increasing water demands, water managers will need detailed snowmelt energy and water balance information from the margin as transitional snow replaces deeper snowpacks.

Further quantification of lower elevation snowline energy fluxes and water balances are needed to identify areas most sensitive to climate change (Bales et al. 2006). For example, decreasing snow water equivalents due to rain in the winter are found at the snowline (Bales et al. 2006), and warmer temperatures and the exposure of soil and rocks in fractional snow cover cause increases in turbulent and radiant heat fluxes (Dozier and

Painter 2004). Due to a "critically limited" number of energy balance monitoring stations throughout the western U. S., Bales et al. (2006) calls for detailed studies of the snow energy balance fluxes and snow characteristics correlated to elevation and latitude.

Snow dynamics and energy balance are generally studied using one-dimensional physically based models. These models use mathematical representations for all of the physical processes controlling energy fluxes to and from the snow. The energy balance is used in conjunction with water mass inputs and outputs to predict melt water production. The point models can be used to in a distributed fashion to improve accuracy over heterogeneous terrain. The more commonly used point models are SNTHERM (Jordon 1991), Simultaneous Heat and Water model (SHAW) (Flerchinger and Saxton 1989), Utah Energy Balance Snow Accumulation and Melt Model, and SNOBAL (Marks and Winstral 2001).

Throughout the semi-arid intermountain west, lower mountain elevations at the snow margin are characterized by shallow patchy snow with a different energy dynamic than deeper snowpacks at higher elevations. Shallow snow can be fully penetrated by shortwave solar energy causing elevated levels of ground heat flux (Baker et al. 1991). Patchy snow, during melt, may receive substantially more of its energy for melt from local advection over adjacent bare soil patches (Zuzel and Cow 1978; Liston 1995).

An understanding of snow packs at low elevations areas at the snow margins is critical as these areas represent the connection between water storage above and water use below. As intermittent and sparse snow packs melt, they participate in a temporal and spatial preconditioning of soil moisture. This soil moisture is critical in establishing hydrologic conductivity between areas of deeper snow and water storage above and

streams and water users below (McNamara et al. 2005). In addition, climatic warming trends will move these snow margins to higher elevations replacing deeper snowpacks and lessening water storage. To better predict these changes in water production, it is necessary to gain more detailed knowledge of the snowmelt energy balance of shallow snow.

Energy fluxes through snow are difficult to measure and model due to their spatial, temporal, and transient nature. The unique components of shallow snow energy, local advection and solar penetration elevating ground heat flux, occur over and through constantly changing snow patches which cannot be measured with traditional weather station measurements in a fixed location. Studies using mobile weather stations have been successful in measuring local advection to patchy snow surfaces. (Granger et al. 2006). However, measurement of ground heat flux below patchy shallow snow has not occurred due to limitations in measurement equipment. Mobile devices are not practical because of the snow disturbance caused by the device. To overcome this problem, an instrument, or many instruments with large spatial coverage, would need to be placed near the soil surface ahead of the snow fall to capture temperature measurements below transient and patchy snow margins occurring in unpredictable locations. With the large spatial coverage of near surface soil temperature measurements, ground heat flux can be calculated beneath the snow patches. This flux information would then complete the energy balance for shallow patchy snow.

Recently a new technology has shown promising results in temperature measurement. Distributed Temperature Sensing (DTS) uses a fiber optic cable to capture accurate temperature readings on large spatial and temporal scales. The technology has a

robust environmental operating range and has been shown to work well in capturing temperatures beneath discontinuous snow packs (Tyler et al. 2008). The study by Tyler et al. (2008) was performed as a preliminary run of the DTS instrument in capturing the interface temperatures beneath shallow snow. The experiment was performed in the foothills of Boise, Id in the Treeline site of the Dry Creek Experimental Watershed (UDCEW). The watershed was a moderate elevation (1604m) semi-arid site with good prospects for intermittent or extended periods of patch and or shallow snow. In the 2008 study, the DTS proved capable of giving relative temperatures and accurately distinguishing between areas of snow and no snow across two aspects of a semi-arid watershed in Idaho. Although these demonstrations have proven the value of DTS technology, few have applied it to snow problems.

In this study, DTS provides point temperature measurements every meter along a fiber optic cable spanning our entire watershed. The point measurements represent the center of the average temperature of a section of cable just over one meter in length. This property will limit the value of direct measurement of a point temperature but is very adept at capturing area averaged soil temperatures beneath transient unpredictable snow patches of differing snow depths. When coupled with heat flux plate measurements, these cable averages allow us to investigate soil temperatures over large spatial extents in complex terrain. Ultimately, these measurements will allow relative comparison of soil temperature between deep and shallow snow.

This study investigates the spatial and temporal variability of ground heat flux beneath shallow patchy snow using DTS. The DTS will allow the measurement of near

surface soil temperatures used to calculate ground heat flux and its contribution to the energy balance of shallow snow.

1.1 Background

Presently, the need to predict anthropogenic changes to climate and the consequent changes to the water balance has drawn attention to the snowmelt energy balance of shallow snow at the snow margin; the area most affected by climate change.

There are three lines of literature relevant to this thesis and the study of shallow snow: studies on the energy balance of snowmelt over unfrozen soil, studies on the unique energy balance of shallow, patchy snow, and incoming solar penetration through shallow snow. These segments of literature are fundamental to the current understanding of shallow snowmelt.

1.1.1Snow Energy Balance

The energy budget for a snow pack volume is

$$\Delta S = \left(Q_{sn} + Q_{li} + Q_{le} + Q_h + Q_e + Q_g + Q_m\right)\Delta t \qquad (1)$$

where ΔS is the change in snowpack energy content (J) during a time period Δt , Q_{sn}, Q_{li}, and Q_{le}, are radiative fluxes of net shortwave (0.3μ-1.2μ), incoming longwave, and outgoing longwave radiation. Q_h, and Q_e, are turbulent fluxes of sensible and latent heat, Q_g, is conductive heat from the soil, and Q_m is advected heat from the snow by meltwater draining from the snowpack. All energy fluxes are in energy per time (J/t). (Marks and Dozier 1992). Water mass contained in the snowpack is accounted for in both the accumulation and melt phases. The mass balance is expressed as the change in water equivalent, ΔW (snow water equivalent, SWE) during a time period Δt and can be written as

$$\Delta W = (P_r + P_s - M_r - E)\Delta t \qquad (2)$$

where P_r, P_s, M_r, and E are precipitation as rain or snow added to the pack and melt or evaporation leaving the snowpack. Figure 1.1 shows a schematic of the energy and mass balances of a melting snowpack.

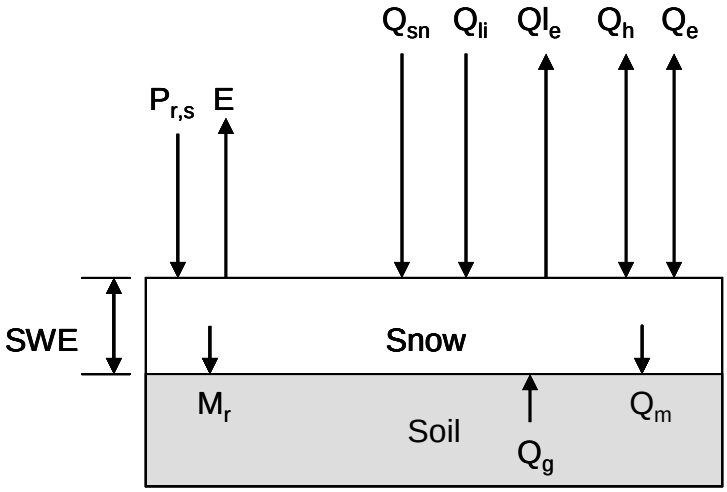

Figure 1.1. Schematic of energy and mass fluxes to and from a melting snowpack.

The study of snowpack energy and mass balances has undergone an evolution. Beginning with a focus on understanding and modeling large energy flux components of mid latitude alpine snowpacks, subsequent studies focused on specialized terrain or minor energy balance components and processes. This evolution or change in focus is outlined in the following paragraphs.

Snowpack energy balance studies focus on the largest energy components, net radiation and turbulent exchange, and generally ignore ground heat flux (Q_g) commonly referred to as G. Zuzel and Cox (1975) found that using net radiation, vapor pressure, and wind (for turbulent exchanges), improved snowmelt modeling 13% over temperature alone; signaling the need for more physically based snowmelt modeling.

Comprehensive snowmelt energy studies emerged confirming net radiation and turbulent exchange as the dominant energy fluxes to deep snowpacks. Despite the deserved cursory treatment, many of these studies allude to the importance of G at certain locations or times or leave the importance of G quietly in the results. During snowmelt at Emerald Lake in the Sierra Nevada Mountains, Marks and Dozier (1992) found radiation provided 66%-90% of the energy for snowmelt with ground heat flux (G) accounting for up to 12% when viewed on a monthly time scale. The authors commented that although G was small, it produced significant melt during midwinter. Cline (1997), investigating a very high elevation site in Colorado (3517m) found net radiation and turbulent fluxes to provide 75% and 25% of snowmelt energy over the winter season. Despite leaving G out of the energy budget, use of a heat flux plate helped verify that ground heat flux was insignificant except at the very end of the melt when snow was very thin. Şensoy et al. (2006) studied high elevation sites at 40° latitude that were frequently very cold with shallow snow covers. Results from the study find net radiation and turbulent fluxes accounting for 70% and 30% of the melt. In addition the authors found that setting the soil temperature to 0°C beneath snow with a temperature less than 0°C gave them an unexpectedly high G. To remedy the unexpected result, they used soil temperatures taken at 20cm depth from a geographically similar weather station.

There are studies that find G to be very important at certain times of the winter or stages of melt. Expressed in graphic but not written form throughout the study by Şensoy et al. (2006) is the fact that G occasionally accounts for over 50% of the 5 day average energy balance. This usually occurs early in the season or later when the snow is 0.5m or less and the weather more volatile with both warm and cold periods. The relative

contribution to the energy balance is particularly pronounced after spring cold spells when the snow pack cools and temperature gradients increase at the warm soil surface, increasing the soil heat flux towards the snow. At a wind sheltered site, G accounted for over 50% of the energy fluxes for one fifth of the 5-day time intervals representing the winter.

At the Reynolds Creek watershed near Boise, Idaho, Marks and Winstral (2001) found net radiation or sensible heat to be the dominant energy source during meltout. At their ridge site, where winds are stronger and snowpacks are thinner, sensible heat flux is the dominant source of melt energy with G equal in magnitude to net radiation and essentially canceling it. This situation results from meltout occurring before the crossover from negative to positive net radiation. Crossover occurs later in spring when sun angles are higher and days are longer allowing the magnitude of shortwave radiation to overcome thermal emission from the snowpack. For the two years during meltout at the ridge site, G as a proportion of energy transferred was 10% and 19%. For the same periods, when considering net radiation, net turbulent, and G as positive contributors to melt, G provides 20% and 82%. This example does not show that G is large in magnitude but emphasizes the importance of G for melt at a time and location characterized by shallow snow and early meltout.

Pomeroy et al. (2003) expressed results emphasizing potential daily values of G. While studying aspect affects on different components of melt energy in the Arctic, heat flux plates measured peak downward values of G exceeded 80W/m^2. The readings followed a melting period where the snow became patchy and shallow. The high value is downward due to the frozen soil below the flux plates. Fluxes of 20W/m^2, directed

towards the snow, followed as a result of thawed ground below the plates and cloudy, cooler conditions cooling the snow above.

Smith et al. (2007) suggests a feedback loop created by the addition of ground heat to the base of the snowpack. The loop shows ground heat creating ground melt which increases soil moisture and soil thermal conductivity. The increased thermal conductivity creates a positive feedback loop increasing the rate of heat conduction to the snowpack. Smith et al. (2007) supports the hypothesis that there is enough G to generate the measured ground melt by demonstrating that at most only 28% of G was needed to produce all of the ground melt. In addition, the study finds that ground heat was responsible for up to 36% of all midwinter melt.

Hawkins and Ellis (2007) followed an observation from a study by Cayan et al. (2001) stating that 10% of the variation in all of the western United States SNOTEL data came from 3 sites in Arizona. To explain this variance, Hawkins and Ellis (2007) demonstrated the difference between the energy budget of commonly studied higher altitude deep snowpacks and the energy budget of shallow transient snow found in the southwestern US. Hawkins and Ellis (2007) found G accounted for up to 18% of the entire ablation period for one site. The relative contribution of G is increased due to shallower snow depths with more atmosphere-ground interaction over several ablation intervals. Climate is responsible for the increased G. In the this region of the southwest, peak SWE is 35 days earlier and final ablation is 54 days earlier than the earliest of all other regions in the western US. For midwinter ablation periods, incoming shortwave is suppressed due to low sun angles and short days. In addition, the arid subtropical air

mass promotes a negative latent exchange through increased evaporation and sublimation, elevating the importance of G in the southwestern US.

Mazurkiewicz et al. (2008) addresses rain on snow events (ROS) and the shows that ground heat flux is an important component of the snow energy balance in the Pacific Northwest. It is important to note that soil temperatures remained above 0°C throughout the water years under investigation. In contrast to the notion, Mazurkiewicz et al. (2008) reports for individual water years, G accounted for 8%-42% and 42%-85% of the energy balance. During ROS events, G accounted for 8%-24% of melt energy. Despite his analysis of G contributions to ROS, and concern for the non-influential reputation of G, Mazurkiewicz et al. (2008) doubts his G calculations due to "some bias" in his soil temperatures, stating the soil temperatures should have been 0°C in the spring due to percolating meltwater.

The majority of snowmelt energy balance studies reviewed are classified as mid-latitude alpine and focus on the energetics of seasonal, persistent snowpacks. At these higher elevations, warm autumn soils are covered early, and gradually cooled throughout the winter. By late spring, sun angles are high and snow ablation progresses quickly through the final stage. In this final stage soil temperatures are near 0°C with melt water removing the remaining temperature gradient and G flux. These studies confirm that G is a minor contributor to the seasonal energy balance of the snow pack but can generate substantial melt throughout the midwinter season. However, previous to final ablation, during rain on snow events, or at lower elevations or latitudes, snowpacks may become, or be characterized as, shallow and patchy at which time the energy balance of melt undergoes fundamental shifts at seasonal, monthly or daily time scales.

A few studies emphasize how a lack of spatially varying soil temperature data from has led to a lack of understanding of the importance of ground heat flux. In a study estimating meteorological variables for distributed snowmelt modeling over the Boise River near Boise, ID, Garen and Marks (2005) found that only 3 of 8 meteorological stations had soil temperature and moisture data. These three locations were between 1764 and 2338 meters elevation indicating season long sustained snowpacks over the soil. Summarizing temperature data from these three sites, soil temperatures were set to 0°C for snowmelt modeling, eliminating the temperature gradient between the soil and snow, essentially setting ground heat flux to 0 W/m^2. This treatment concurs with Mazurkiewicz et al. (2008) who states that the importance of ground heat flux is often ignored due to a lack of soil temperature measurements. Garen and Marks (2005) go on to conclude that site location is as important as the variables measured. For the Boise watershed in particular, the limited and high elevation range of data created difficulties with variable interpolations over the watershed with an elevation range of 1000-3200m. This limitation also suggests a lack of data from lower elevation areas with transient snow.

1.1.2 Modeling of Ground Heat Flux

Many methods for modeling G use a vertical temperature gradient in the soil. Heat flux plates can measure ground heat flux directly but not at the soil surface. Measured ground heat flux at the soil surface is typically derived from ground heat flux measured with heat flux plates, soil temperature, and soil properties at specified depths. Commonly, the soil temperature gradient is recorded as the difference between a near

surface temperature and a temperature taken at a depth where the diurnal signal is dampened. Soil down to the dampening depth is referred to as the active layer.

There are many models available for calculating G from soil and snow temperatures and conductivities; however, all are based on the equation for one-dimensional steady state heat flow for a homogenous soil media

$$G = K\frac{dT}{dz} \tag{3}$$

where K is the soil conductivity and dT is the temperature change over distance dz.

There are several ways of estimating a temperature gradient between the soil and snow. The upper temperature can be of the soil or snow, either near the soil-snow interface. The lower temperature measure is usually taken at the diurnal dampening depth in the soil. At the dampening depth, the soil temperature remains at the theoretical annual average temperature of the air at the soil surface and is not subject to diurnal fluctuations. On an annual scale this is true, but when considering a melt period of a few days, weeks, or even months, this annual average temperature does not represent the true temperature at depth. Figure 1.2 reveals the diurnal dampening occurs between 30cm and 45cm depth for the time period of interest and location in this study. The depth of soil temperature measurement was of particular interest in this study as our measurements were taken between 1 and 3cm depth. This depth is relatively close to the surface compared with other studies accounting for ground heat flux. Also important to this study was the use of both soil and snow temperatures in establishing the temperature and the inclusion of vapor flux in the heat conductivity of the soil. All of these factors are included in a model for ground heat, with alterations, used by Marks and Dozier (1992), the method selected for this study.

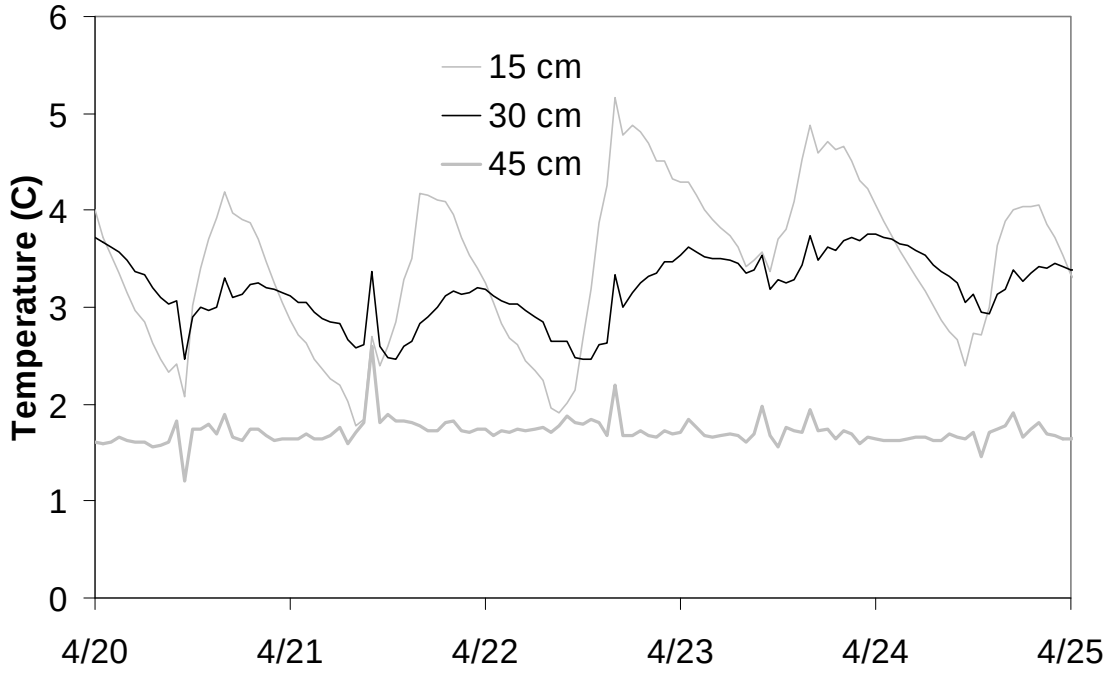

Figure 1.2. Plot shows a dampening of diurnal temperature fluctuations between 30 and 45cm depth. This represents the lower extent of the active soil layer. The instantaneous spikes in temperature are due to instrument noise and do not reflect temperature variations in the soil due to surface processes.

Vapor flux can significantly affect soil heat conductivity. For frozen soils, Chung and England (2006) showed that late winter and early spring ground flux can increase the snowpack energy by 17%. They further concluded that despite air convection and vapor diffusion being 10-7 of conduction, vapor fluxes can be large when soils are unfrozen and wet; indicating that vapor diffusion and G increase for unfrozen soils. This finding further supports the formulation for G (Marks and Dozier 1992) which takes into account vapor diffusion in both soil and snow thermal conductivities.

When considering the importance of various energy components, temporal scale can obscure the relative importance of heat fluxes. Long-term averages can dilute the magnitude and importance of fluxes at different times. Marks and Dozier (1992) note

that hourly average energy fluxes can be greater than +500 W/m^2 despite daily averages rarely exceeding + 200 W/m^2. For example, radiation as the largest percent of the annual snow energy balance is true only if snow ablation continues into late spring when sun angles are higher and days are longer (Mazurkiewicz 2008). This notion is supported by Marks and Winstral (2001) with their crossover concept when net radiation shifts from negative to positive in spring. In the literature, monthly ground heat flux values of 1-14W/m^2 are often reported (Table 1.1). Less often are reports of the percentage of monthly positive flux these values represent which can be as high as 100% (Marks and Dozier 1992; Smith et al. 2007). At these times, such as throughout mid-winter, groundmelt is the only melt taking place and is attributed solely to groundheat.

Table 1.1: Snow energy and mass balance studies including a range of G values, G as a percent of total energy flux, elevations, soil or landscape type, and method of G calculation.

G W/m2	% of total Q	Elevation	Soil or lanscape	Method	Authors
7-1	1-12	3085	Gravel, sand	Calculated	Marks and Dozier 1992
8-1	1-17	2800	Meadow	Calculated	Marks and Dozier 1992
0-4.6	-	500	Lacustrine farm	Measured	Pomeroy et al. 1998
5-14	-	2097	Sagebrush Steppe	SNOBAL	Marks and Winstral 2000
0-14	-	2061	Aspen/Fir grove	SNOBAL	Marks and Winstral 2000
>10	1	2112	Steppe	SNOBAL	Şensoy et al. 2006
1-5	17	-	Steppe	SYNTHERM	Chung and England 2006
6-1	1-18	2325	Ponderosa	SYNTHERM	Hawkins and Ellis 2007
6-19.5	-	1455-1765	Arizona	G=Kdt/dz	Smith et al. 2007
-	8-85	1018-1294	Pacific NW unfrozen	SNOBAL	Mazurkiewicz et al. 2008
-	8-24	1018-1294	Rain on snow	SNOBAL	Mazurkiewicz et al. 2008

Shallow snow develops from local conditions and has an energy balance different from deeper snowpacks. When snow is patchy, local advection dominates the melt energy. When snow is shallow, below 10cm depth, solar radiation can penetrate the snow and warm the underlying soil generating significant additional ground heat flux to the snow (Baker et al. 1991).

Shallow patchy snow can develop through differential accumulation or melt or both. This patchiness usually occurs early and late in the snow season and has been

documented in a variety of environments including arctic and alpine tundra, grasslands, under forest canopies, and the arid Southwest (Marsh 1999; Hawkins and Ellis 2007).

Differential accumulation can be attributed to orographic effects, canopy interception or drifting up until the time of peak SWE (Blöschl and Kirnbauer 1992; Luce and Tarboton 2001) For open complex terrain, differential melt results from the topographic features slope and aspect. In the western US, storm patterns typically scour southwest facing slopes while depositing on northeast facing slopes.

Slope can cause variations in incoming and reflected solar. Aspect can affect albedo and exposure to direct incoming solar radiation. The melt patterns in the western US, loosely defined by north and south facing aspects, result from thinner patchy snowpacks on southwest slopes receiving the most radiation for melt. As snow depth recedes, terrain features such as bushes, rocks, and bare soil, with their reduced albedo, promote small scale differential melt resulting in patchiness on individual faces.

When viewed at scales below approximately 8km, dominant radiation and regional scale advection are overcome by local advection from adjacent snow free soil and vegetation (Liston 1995). Bare ground or vegetation, with albedo ranging from 5%-30%, can heat to temperatures far above the 0°C limit for snow (Grey and Male 1981). This additional sensible heat is then transferred downwind to an adjacent snow patch at a rate declining with distance from the leading upwind edge of the patch (Essery et al. 2006). As an example of how local advection shifts the energy balance, Zuzel and Cox (1978) note that over a continuous snow surface, 60% of melt energy is from net radiation, but over a single snowdrift, 60% of the melt energy comes from advected heat radiated just from the surrounding bare soil and vegetation.

Liston (1995) modeled the surface energy balance over patchy snow finding up to a 30% increase in convective melt energy but his surface model intentionally disregards snow depth and ground heat flux. Olyphant and Isard (1988) found that increasing wind speed resulted in modeled increases of 138-347W/m^2 of available sensible heat from snow free patches to the leading edge of a snow patch. At 1000m from the leading edge, additional sensible heat was reduced to 58W/m^2. These values compared to calculated net radiation values of 93-138W/m^2. The modeled results differ from their empirical estimates of less than 1 W/m^2. In a field study on advection by Neumann and Marsh (1998), ground heat flux plates were not installed below the snow patch, therefore G was not included in the snow patch energy balance.

1.1.3 Solar Shortwave Radiation Penetration of Shallow Snow

Visible light in the wavelength band 0.3 -1.2μ, penetrates shallow snow providing energy to heat the underlying soil resulting in increased heat conduction (G) to the snow (Baker et al. 1991). The magnitude of light penetrating the snow follows a characteristic extinction curve with increasing snow depth (Figure 1.3). Therefore, as the snow depth decreases, greater solar inputs to the soil are expected to increase surface soil temperatures and melt.

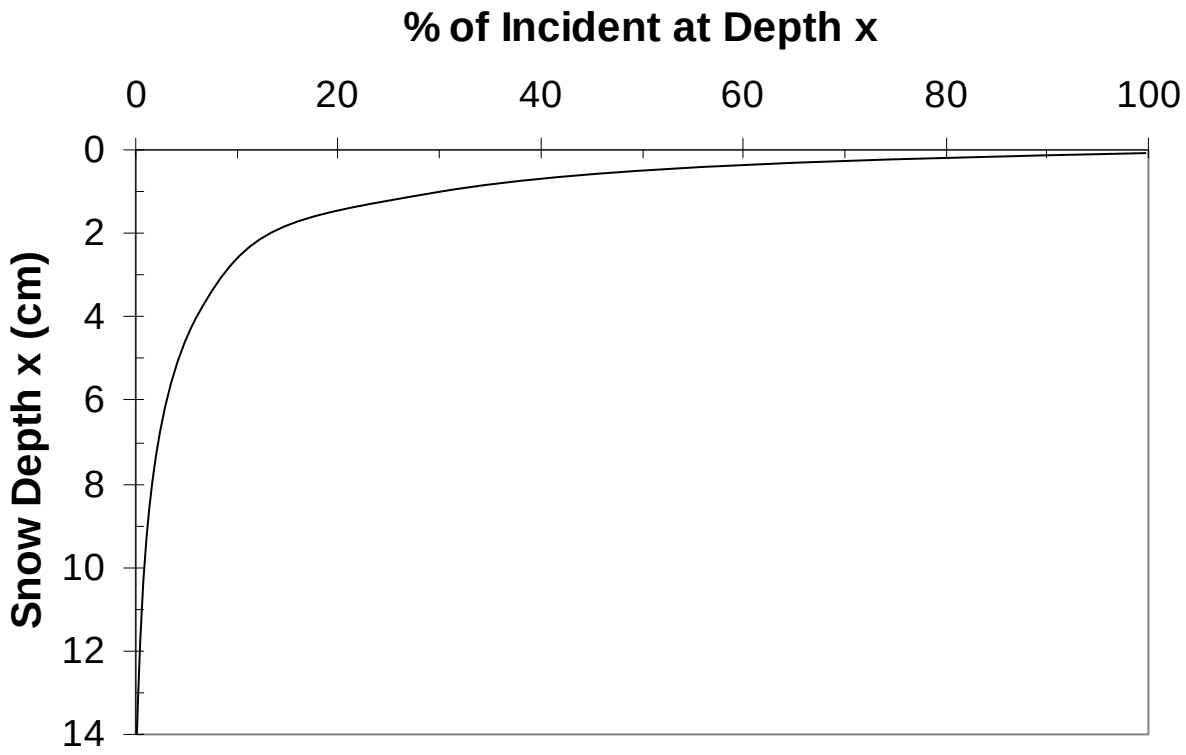

Figure 1.3. The figure adapted from O'Neill and Grey (1973) light extinction through the snow surface as the percent of incident light reaching a given depth. The light is wavelengths 0.3μ-1.2μ.

Solar radiation penetrating snow less than 10cm in depth, is absorbed, and conducted back into the snowpack (Baker et al. 1991). The snow is porous so the reflectivity occurs not at the surface but throughout near surface depths of 5-100cm (Baker et al. 1991). More important is the percent of incident radiation to the snow surface that reaches the ground resulting in increased soil temperatures.

The amount of shortwave radiation reaching the soil shares a coupled relationship with snow albedo (O'Neill and Gray 1973). During the melt period, snow albedo can range from 0.85 to 0.45 for new and old snow surfaces. After a quick decline in albedo within 2-3 days, the albedo follows a decreasing rate of change as the snow surface ages (Dingman 2002). In addition, solar penetration increases with snow grain size allowing a

larger proportion of solar energy to penetrate as the snow ripens (O'Neill and Gray 1973). A snow surface albedo of 70% is considered the minimum to negate surface albedo reduction from underlying dark plant or soil surfaces (O'Neill and Gray 1973; Baker et al. 1991). To re-phrase, once the snow albedo is above 0.7, underlying plants and soil no longer affect snow surface albedo. Translating this to snow depth, Baker et al. (1991) used plant cover to categorize the masking depths and found 5.0, 7.5, and 15cm for bare soil, sod, and alfalfa.

Figure 1.3, adapted from O'Neill and Gray (1973), shows the percent of surface radiation (0.3 -1.2μ) that reaches a given depth of snow. For a black surface, 40% of incoming solar will reach the surface below 1cm of snow and 3%-4% will reach the surface below 10 cm of snow. For solar energy levels sufficient to raise soil temperatures, 10 cm is the accepted maximum depth (Baker et al. 1991).

To capture and compare the effects of solar penetration on soil temperatures, it is necessary to measure soil temperatures beneath undisturbed snow greater and less than 10 cm depth. During spring melt, shallow snow is unpredictable due to its transient nature in space and time. A point measurement may capture soil temperatures below various depths of snow but, not at comparable times. To make a reasonable comparison between deep and shallow snow, many point measurements would have to be made beneath unpredictable snow conditions and locations simultaneously. As a solution to this problem, recent DTS technology has offered high spatial resolution temperature measurements derived from a watershed scale length fiber-optic cable placed just under the soil surface previous to snow fall. The cable can measure soil temperatures from multiple locations at the same time.

1.1.4 DTS Theory

Capturing temperatures at the snow/soil interface can be done at the point scale which may not represent variations over time and space. Conditions at the snow/soil interface can vary with many variables such as time, snow depth, aspect, and environmental conditions. Recently, Distributed Temperature Sensing (DTS) has emerged as a technology capable of large spatial applications in environmental research. Soil/snow interface temperatures (Tyler et al. 2008), groundwater borehole logging, groundwater/stream interactions, physical limnology studies, and atmospheric profiles (Selker et al. 2006) represent the variety of current uses for DTS. The advantage for all of these applications is the high temperature and spatial resolution not possible with traditional hydrologic instruments.

DTS receives accurate temperature measurements with high spatial resolutions from common fiber-optic cable over distances up to thirty meters. The technology is based on Optical Time Domain Reflectometry (OTDR) where pulses of laser light are sent down the cable, reflected back, and sensed to calculate temperature and location. With this technology, high resolution, 1m, 10s, and 0.1°C snow soil interface temperatures enable a detailed study of the snow-soil interface temperatures over varying areas of complex terrain throughout the winter and melt periods.

Physical properties of the cable including refractive index and the silica molecular lattice, are used to calculate temperature, location along the cable, and the spatial resolution of the measurement. Light pulses are sent down the length of the cable. The light energy excites the lattice structure and silica molecules of the fiber causing the structure to vibrate. This vibration scatters the light sending several forms of backscatter

back along the same path within the cable. The Raman backscatter used to calculate temperature has two components. A Stokes signal is returned with a wavelength greater than the incident light which is stable with respect to temperature and an anti-Stokes return has a wavelength lower than the incident light and is responsive to temperature. The ratio of anti-Stokes to Stokes has a linear relationship to temperature and is used is calculating a raw temperature reading. The raw temperature readings, or return signal, are altered by a linear attenuation of signal along the fiber and by discrete losses of signal from the system, cable connections, or damage to the fiber. Through a variety of calibration techniques using know temperatures, the raw signal data is corrected and converted to actual temperatures. Details of the calibration used in this study are given in the methods section of this thesis. The following paragraphs explain how the DTS takes measurements and follow the examples from (Smolen and van der Spek 2003).

The location of measurement along the cable is determined by the round trip time of the light pulse and the speed of light in the cable. First the light velocity of the cable is determined by dividing the speed of light by the refractive index of the cable. The unitless refractive index for the glass in our cable is ~1.5 (1.46). The speed of light in the cable is therefore ($3x10^8$ms)/1.5 or $2x10^8$m/s. The distance to a point on the cable, is half of the round trip time of the outgoing light pulse and backscatter multiplied by the speed of light.

The temperature measurement along the cable is taken using the average temperature of the cable over the spatial resolution set by the user. In this study, a 1m spatial resolution was set. This means that the temperature readings are the average temperature of each 1m section of cable, centered over the respective 1m sections. The

1m spacing is controlled by a shutter accepting the incoming scattered light. The shutter is open for a length of time necessary to capture one meter (z) of light. The open shutter time is determined by dividing the round trip time of a meter of light by the speed of light in the cable. Therefore, the open shutter time is $(2*1m)/2x10^{8}m/s$, $10^{-8}s$, or 10ns.

The temperature measurements are taken continuously and averaged over a period of time set by the operator. The accuracy of temperature measurement is a trade-off between cable length and measurement time. A shorter cable will give a more accurate temperature measure. A longer averaging time will give a more accurate the temperature measurement. These tradeoffs are expressed in Figure 1.4. This study used a short 375m cable, and a long, hourly averaging time to achieve temperature accuracies of ± 0.03˚C.

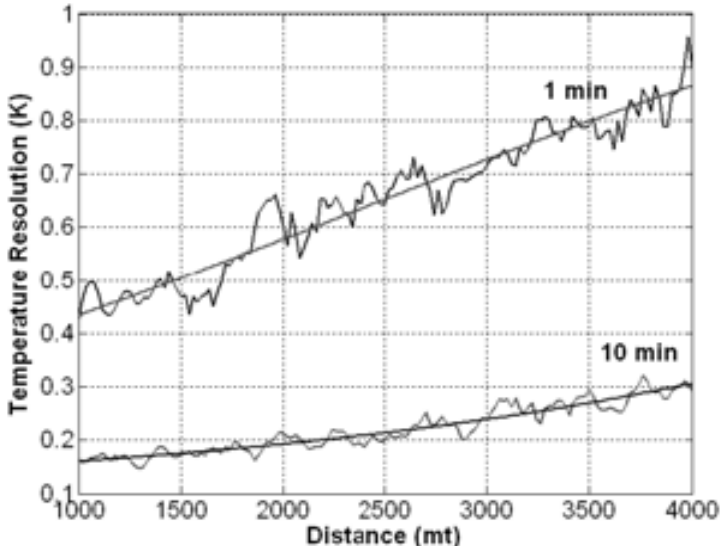

Figure 1.4. Temperature resolutions (exponential fit) of the DTS for 1 and 10 minute averaging times for up to 4 km of fiber-optic fiber. (Soto et al. 2007).

How the Agilent DTS records point measurements is fundamental to spatial accuracy. To report the measurements, the Agilent averages temperature over one spatial scale while reporting at another. In this study, the spatial resolution of the averaging (light pulse width) and reporting were set at one meter, the finest setting. The point measurement is centered over the pulse width. However, the pulse does not have sharp

edges and uses temperatures found about 0.1m past the ends of the 1m light pulse. This has two implications: first, if you are trying to measure the temperature of a target that is not a full meter wide, the DTS will average in temperatures from outside your target and second, temperatures are taken slightly beyond the pulse width so there will be influences in your temperature measurement from outside the specified pulse width. For the Agilent machine, meter 0 is at the connection to the DTS machine (Dorighi 2009a). When using a DTS it is very important to consult the manufacturer on specifications for the averaging properties as the tapered averaging can greatly affect measurement.

In March of 2007 the DTS was tested in the Treeline site to assess the capability of the instrument for measuring snow/soil interface temperatures beneath varying snow cover in complex terrain. Initial results were promising and led to the justification of the present study. The publication of this work (Tyler et al. 2008) includes two similar studies: one done by a team in Mammoth, California and another done in Boise, Idaho. The following paragraph summarizes the findings of the two studies in the publication. Two similar studies were performed in different locations testing DTS capabilities in capturing snow soil interface temperatures. In a late-spring study at Mammoth Mountain, California, a 24 hour effort using 330m of fiber-optic cable produced temperature accuracies of 0±0.2°C using 10s averaging (Tyler et al. 2008). Of note at the mammoth Mountain site was the lack of damage to the cable after being buried for the entire winter and temperatures recorded as high as 40°C where the cable was snow free, exposed on the soil surface. Tyler et al. (2008) also highlights a similar study occurring at the same time at the Treeline site in the foothills outside of Boise Idaho. In the Idaho study, 36 hours of DTS data were collected from an 85m section of fiber-optic cable

buried just beneath the soil surface. The cable captured the differential melt occurring on opposing North and South facing slopes following a 50cm late-season snowfall. The DTS proved effective in capturing conditions beneath unpredictably located patches of snow and showing differential melt patterns due to the effects of solar heating on the opposing slopes.

1.2 PROBLEM STATEMENT

At lower latitudes or elevations, regional air masses or local climates can create seasonal conditions characterized by persistent or transient shallow snowpacks with unique a unique energy balance (Figure 1.9). In these areas, the relative importance of ground heat flux may differ from high alpine snow energy balances on seasonal or monthly scales (Yenko 2003). For single events, Mazurkiewicz et al. (2008) showed G to be significant despite large amounts of meltwater infiltration beneath the snowpack. At daily scales, Pomeroy et al. (2003) demonstrated ground heat flux to be very high following a period of rapid ablation. These studies represent a recent interest in ground heat flux beneath shallow snow or report unexpected or unusual ground heat flux values found at a time when shallow or patchy snow was present. None of the studies address the range of ground heat flux values found as snow depth recedes from deep, >10cm, to complete ablation. According to the light extinction curve (Figure 1.3), it is likely there is a measurable soil temperature response below snow up to 2cm depth with a rapidly decreasing effect below 2 to 10 cm snow depth. Because there is little documentation of ground heat flux values under shallow snow, doubt is often cast when measured or modeled values for ground heat flux exceed those found in the literature.

The objective of this study is to compare ground heat flux beneath snow less than 10 cm depth (shallow) and greater than 10cm depth to see if solar penetration of shallow snow results in the heating of soils and an increased ground heat flux. Further objectives of the study are to evaluate the mathematical model for ground heat flux and to assess the DTS as a tool for measuring soil/snow interface temperatures beneath spatially unpredictable shallow snow extents.

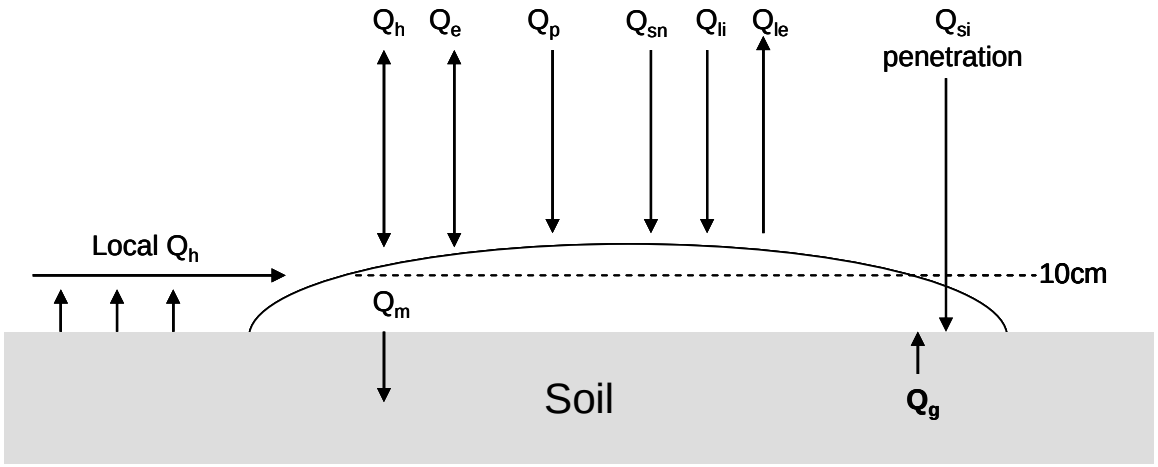

Figure 1.5. Conceptual model of shallow patchy snow energy balance. Q_{sn} is net short wave radiation; Q_{li} is incoming longwave radiation; Q_{le} is outgoing longwave radiation; Q_{si} penetration is incoming shortwave radiation penetrating snow depths ≤10cm; Q_p is advected energy from precipitation; Q_g is ground heat flux; Q_h is sensible heat; Q_e is latent heat; Q_h local is advected heat from warm bare soil patches upwind of a snow patch; and Q_m is heat advected from the snow by meltwater draining from the base of the snowpack. The 10cm line represents the maximum penetration depth of solar radiation.

2. STUDY SITE

2.1 Study Site

2.1.1 Site location

The Dry Creek Experimental Watershed (DCEW) was established in 1998 by the Agricultural Resource Service and Boise State University to investigate watershed processes. The watershed is situated in the Foothills to the north of Boise, Idaho (Lat: 43° 34'N, Long: 116° 14'W) which represent the southwestern extent of a mountain range that extends the Rocky Mountains to the Canadian border. The DCEW is represented by four experimental sites at four elevations: 1151m, 1640m, 1700m, and a SNOTEL site at 1932m. The lowest site is primarily snow free throughout the winter whereas the upper two sites experience deeper persistent snowpacks throughout the winter. The remaining site at 1640m is characterized by intermittent snowpacks therefore offering the greatest opportunity for capturing the characteristics of shallow, patchy snow.

The Treeline site at 1640m is a 0.02km^2 sub basin of the Dry Creek Watershed (Figure 2.1). The watershed has three ephemeral streams with a central intermittent stream splitting the watershed and draining to a southeast azimuth of 139°.

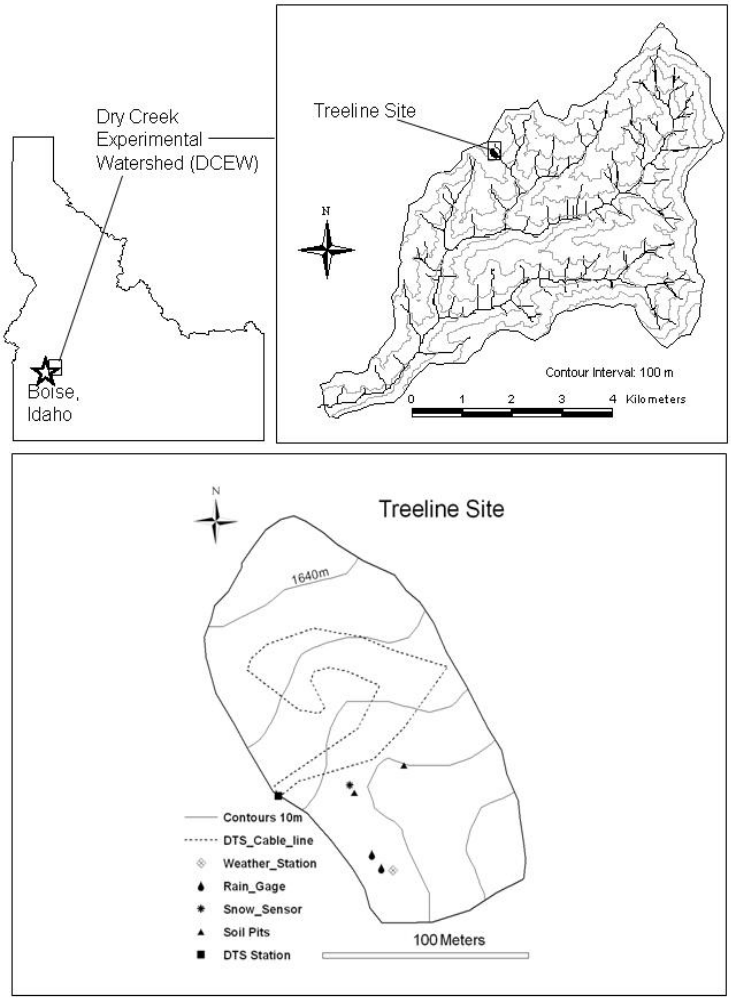

Figure 2.1. Treeline watershed site map.

2.1.2 Soils

The Treeline site has sandy loam soils with properties listed in Table 2.1. It is important in this study to note that soils drain very quickly and overland flow does not occur. In addition, because of the lower elevation of the site, soils can remain unfrozen under the snow, or frozen in years when the there is little snow and soils are exposed to freezing air temperatures.

Table 2.1. Soil properties for Treeline (Gribb et al. 2009).

Soil Properties	g/cm^3		%					
Soil Depth (cm)	Bulk Density	Particle Density	Gravel	Course Sand	Fine sand	Silt	Clay	Porosity
0-24	1.5	2.6	22	55	16	5	2	0.38
24-52	1.5	2.6	25	53	16	5	1	

2.1.3 Climate

Pacific maritime air masses drive the precipitation regime for the Boise region. The majority of precipitation is delivered between December and June by northwest winds and cold fronts originating from the Aleution Low (Williams 2005). Treeline receives an annual precipitation of 57cm, intermediate between Boise (31cm) on the valley steppe below and approximately 100cm at the forested Bogus Basin SNOTEL site above (Williams 2005). In summer, a Pacific high pressure system dominates the region with occasional thunderstorms temporarily relieving very dry conditions.

The Treeline site is situated between 1600 and 1650m. This elevation marks the start of an ecotone where the sagebrush-steppe gives way to the coniferous forests above. The sagebrush-steppe has a Köeppen classification of BSk indicating an annual average temperature below 18°C, with at least one month averaging below 0°C, and annual average precipitation of 25-50cm (10-20 inches). A climatograph for Boise is provided in Figure 2.2. The Treeline site receives an annual precipitation of 57cm which provides sufficient conditions for coniferous trees to take hold. Therefore, the Treeline has 9% canopy coverage during the winter season provided by 18 Ponderosa Pine and Douglass Fir trees (NOAA 2001).

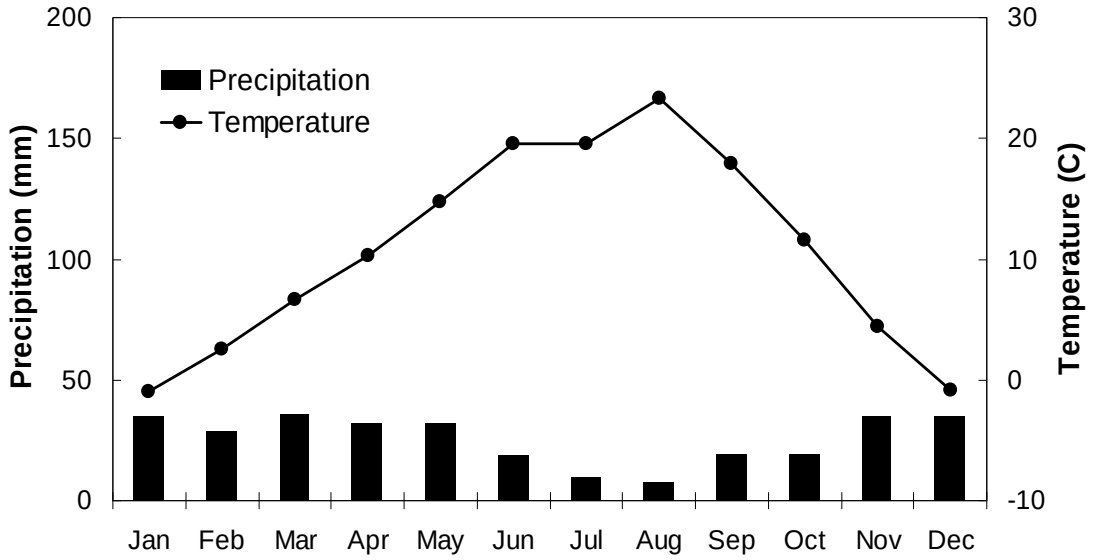

Figure 2.2: Climatograph of average monthly temperature (Line) and precipitation (Bars) from 1971-2000 for Boise, Idaho, elevation 858m (2008).

2.2 Snow Year 2008-2007

The winter of 2007-2008 was average for the mountains and above average at the Treeline site. Figure 2.3 shows a SWE history from the National Resource Conservation Service (NRCS) Bogus Basin snow survey site approximately half a mile from, and at the same elevation as, the Treeline site. March 1 SWE for 2008 is the 6th highest on record. The deep snow, cold temperatures, and intermittent snow storms extended the snowmelt with April 22 as the final meltout day for the watershed.

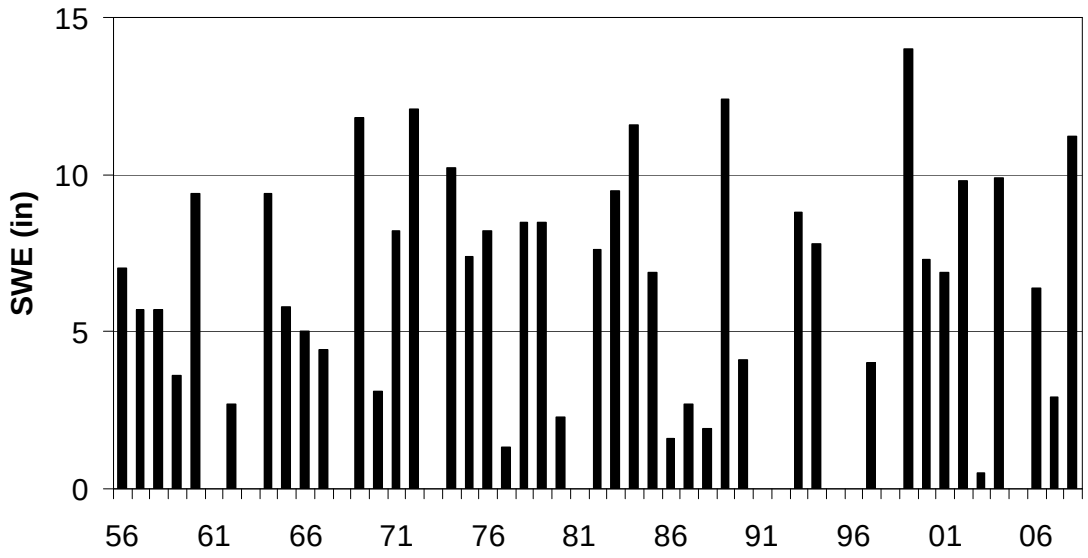

Figure 2.3. NRCS Bogus Basin snow course March 1 SWE measurements for 1956-2008. The 2008 winter brought the sixth largest SWE measurements ever recorded at this lower elevation. Adapted from NRCS (2008)

3. METHODS

The Treeline site provided an optimum location and size, with its moderate 6400m elevation to capture the energy dynamics of shallow snow. A DTS system was deployed throughout the watershed to capture soil/snow interface temperatures. The DTS measurements provided ground heat flux to complete weather data logged hourly by a permanent weather station and soil pits. One soil pit was outfitted with two heat flux plates to validate G calculations from DTS output. Snow surveys were used to track snow depth and SWE for the entire melt period. After complete meltout in late April, the DTS cable was removed from the watershed for calibration.

3.1 Snow Surveys

3.1.1 Basin SWE

Surveys of snow depth and snow water equivalent (SWE) were performed weekly throughout the snowmelt season at thirteen sites chosen for redundant sampling of representative aspects and slopes (Figure 3.1). Sample point selections, equipment, and techniques follow the recommendations found in Grey and Male (1981). The authors suggest that five samples, no more than 30m distance between samples, be taken at each site. Due to the small size of the watershed, three samples were taken within 1m at each site with sites no more than 50m apart.

3.1.2 Transect Depth Measurements

When snow patches developed over the fiber-optic cable, transects were set up over the snow above the cable. Daily snow depth measurements were taken along the string transects over the snow patch (Figure 3.1). Marks were made on the string every half meter with whole meter marks coinciding with meter marks on the DTS cable below the string. A 4mm rod was inserted into the snow to measure depths with an accuracy of 0.5cm. The holes had very little to no effect on the melt rates as evidenced by the lack of surface cupping around the holes and the holes being present with less than 0.5cm of snow on the ground.

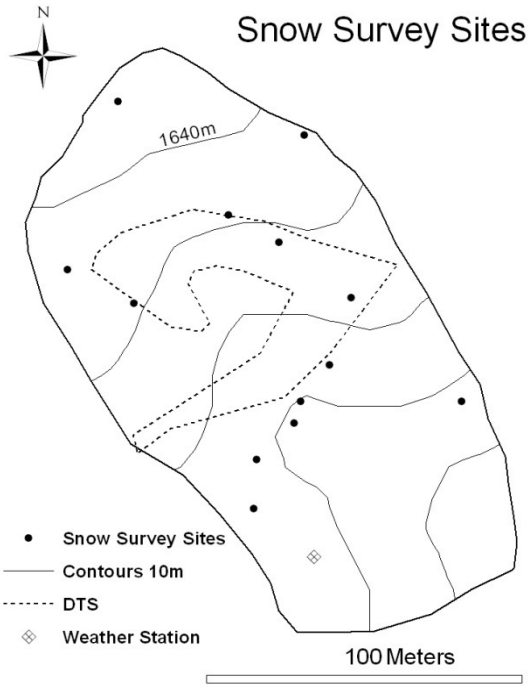

Figure 3.1. Thirteen points used for weekly snow surveys. The points were chosen to represent redundant sampling for all faces and slopes in the watershed. DTS Fiber optic-cable placement yielding snow-soil interface temperatures.

A Federal Snow Sampler was used to take samples of snow depth and SWE at the thirteen sites. At each site, three samples were averaged for depth and SWE. If the snow depth is below 25cm, the three samples were weighed together in a plastic bag. In addition, the average of two depths were taken every 3 meters from one site to the next using a Life Link metric snow probe. Basin averaged SWE had a maximum of 22.4 cm on February 13 with the final melt on April 22 (Figure 3.2).

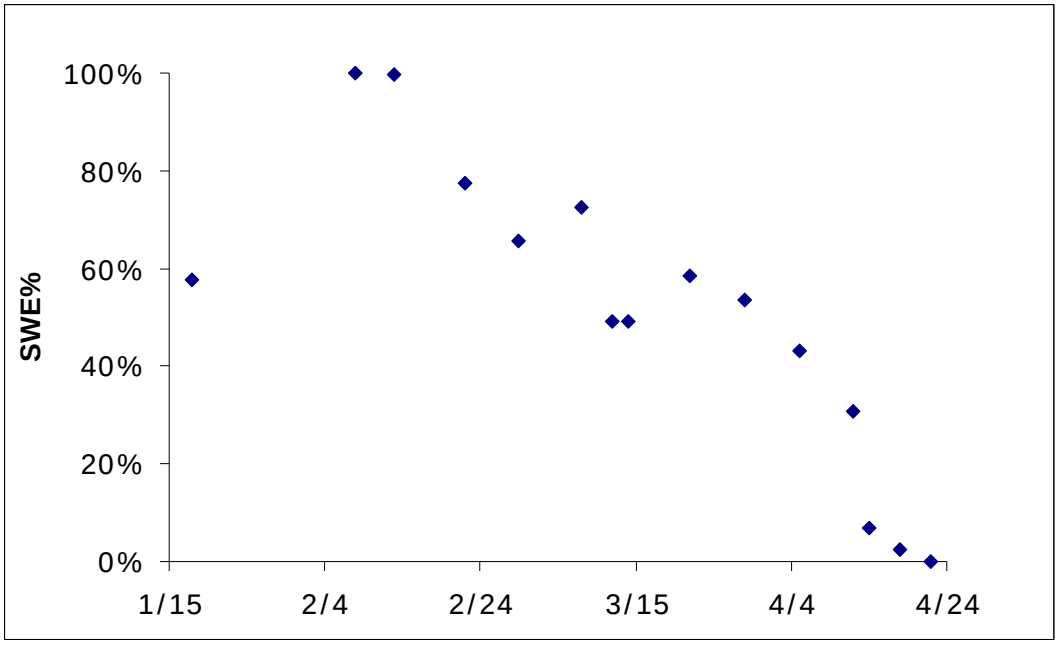

Figure 3.2. Measured basin average snow water equivalent normalized to maximum SWE of 22.4 cm.

3.2 Meteorology

3.2.1 Instrumentation

The Treeline watershed has an instrumented weather station and several instrumented soil pits on the two primary aspects. A distributed temperature system was used to log soil-snow interface temperatures throughout the watershed. See Table 3.1 for specifications on all of the instruments used in this study.

Table 3.1. Specifications for meteorological and soil instruments used in this study.

Instrument	Range	Accuracy
Campbell CR10XTCR Thermocouple Reference T	-35 to 50°C	± 0.5°C
Belfort 5915-12 weighing bucket raingage	12 in	± 0.5%
03101 R.M. Young Wind Sentry Anemometer	0 to 50 m/s	± 0.5 m/s
Campbell CS215 Temperature and RH Probe	0 to 100%	± 2%
Campbell CMP3 Pyranometer	0.3 to 2.8µm	± 5%
Agilent N4385A Distributed Temperature System	-10° to 60°C	± 0.03°C
Campbell HFT3 Soil Heat Flux Plates	± 100 W/m^2	± 5%
Campbell CS615 Water Content Reflectometer (VWC)	0 to 50%	± 2.5%
Traceable 4000 Digital Thermometer	-50 to 150°C	± 0.05°C

3.2.2 Precipitation Data

Precipitation data for 2008 was gathered using a weighing bucket rain gage and processed using the Automated Precipitation Correction Program (APCP) (Nayak 2008). Precipitation was logged at 15-minute intervals from a bridel shielded Belfort 12 inch capacity weighing-recording rain gage 2 meters above the ground. Using the APCP, electronic and wind noise, decanting effects, and out of range values were removed from the precipitation data. APCP filtered data was then wind corrected using the program DFIR Intercomparison Shielded Gage (Figure 3.3) (Yang et al. 1998). The program accepts hourly inputs of precipitation data (mm), wind speed (m/s), and temperature (°C). Precipitation is first classified as rain, mixed, or snow, based on critical temperature

settings. The upper temperature limit of 3°C defines all precipitation as rain and a lower limit of 1°C defines all precipitation as snow. Any precipitation falling between these limits is considered mixed rain and snow. In the current time-step, the program uses the temperature classification to choose one of three equations for the adjusting calculation. The wind correction formulas are those for shielded gages (Campbell 2003). Because the only factor in gage under-catch is wind speed (Yang et al. 1998), in each time-step, only precipitation class, wind speed, and precipitation average are used to calculate the wind correction for a shielded rain gage.

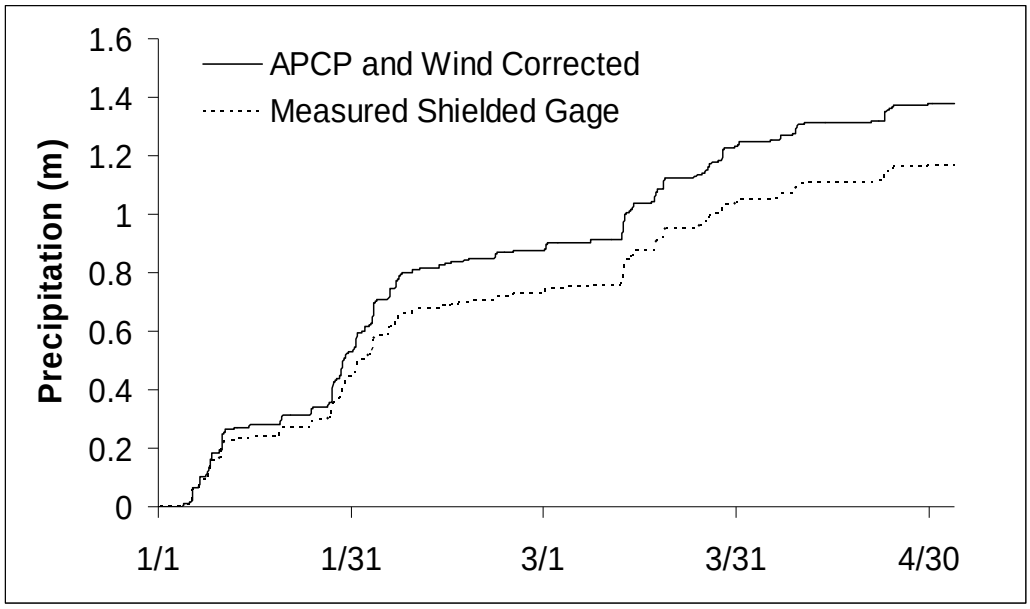

Figure 3.3. 2008 noise and wind corrected precipitation for the Treeline shielded rain gage.

3.3 DTS

3.3.1 Soil-Snow Interface Temperatures

To assess ground heat flux through time and space, a high resolution Distributed Temperature System (DTS) was deployed to capture soil-snow interface temperatures. These temperatures and depths of measurement were later used to calculate G.

The DTS has two components: a multi-mode optical fiber cable (Kaiphone Technology Co., ltd, 50/125 PE Jacketed Armored Optical Fiber Cable) that responds to temperature and an Optical Time Domain Reflectometer (Agilent Technologies N4386A) that detects temperature along the cable length. To capture snow-soil interface temperatures, 375m of fiber-optic cable were buried an average depth of 2.5cm beneath the soil (Figure 3.4) covering all aspects and slopes of the UDCEW (Figure 3.1). The DTS uses light pulses to measure temperatures every meter along a fiber optic cable with an accuracy of ± 0.03°C.

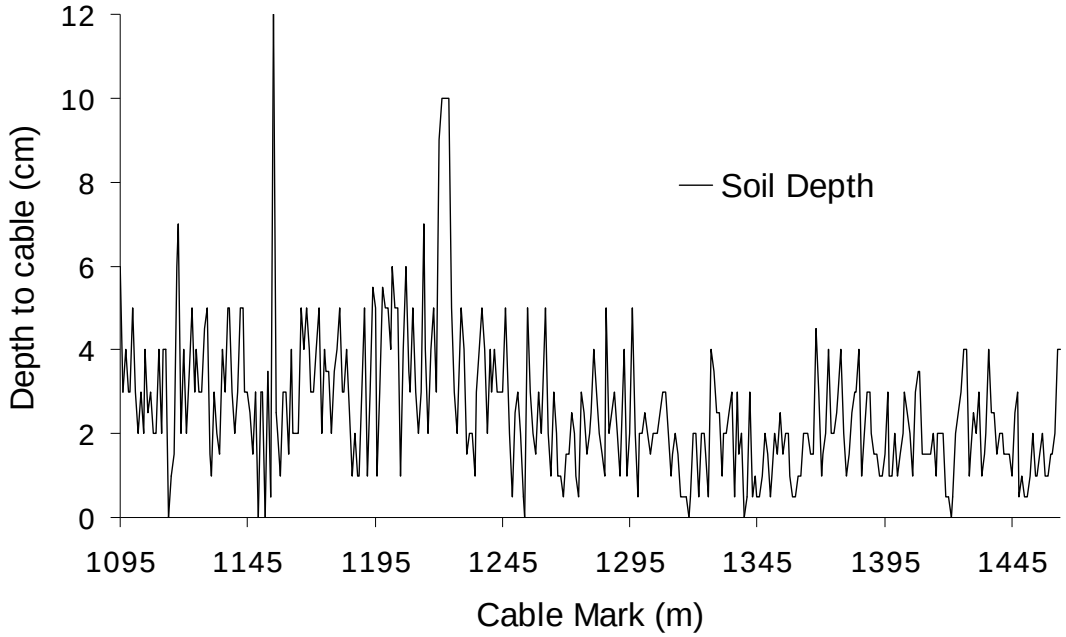

Figure 3.4. Burial depth for 375 meters of DTS fiber-optic cable used for sampling snow-soil interface temperatures. The cable marks represent measurement locations not absolute distance from the measuring device.

3.3.2 Calibration of DTS

Fiber optic cable and the connectors on each end of the cable have unique properties. The cable has a natural attenuation of signal as a function of distance from the signal source/receiver and requires a correction. The connectors introduce a discrete loss of signal. For this study, the two connectors reside between the signal source/receiver and the origin of the cable used for the measurements. Therefore the connector losses are consistent for all temperature measurements. The DTS system, source/receiver, cable, and connectors, require a temperature correction to "offset" the loss of signal that is consistent for all temperature measures beyond the point of discrete loss.

Calibration of the DTS cable was complicated by damage to the cable. At approximately 90m out on the cable, rodents had chewed the cable to the inner sheath

without breaking the glass fiber. This damage created two discrete sections of cable each with unique but consistent properties requiring separate calibrations of attenuation and offset (Dorighi 2009b). This damage appears as a break in slope of the raw temperatures (Figure 3.5). The calibration was performed in three steps after the cable was extracted from the soil on April 22, 2008.

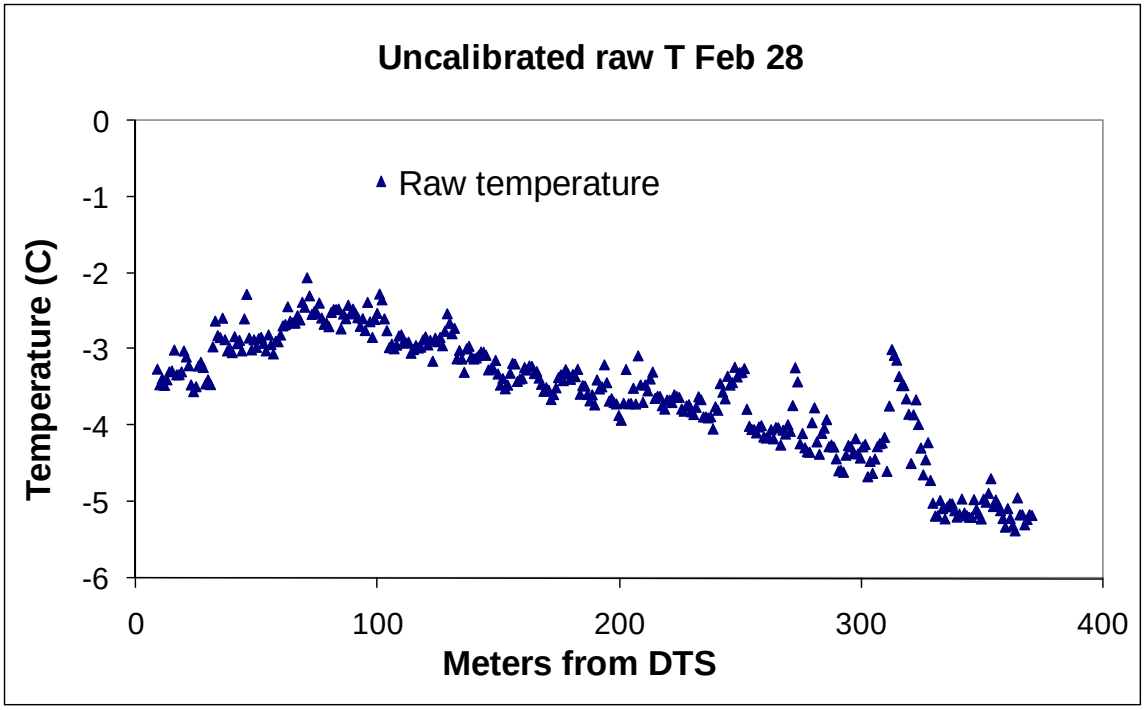

Figure 3.5. February 28 raw temperature trace (uncalibrated) for 370 meters of cable under uniform conditions and negligible melt. The break in slope represents damage to the cable at the break.

Initial calibration of the DTS cable for attenuation and offset was performed using a single ended DTS measurement with a dual bath method. Two eleven meter sections of the 550m field fiber-optic cable were placed in two water baths of 17.58°C and 20.95°C respectively. The two calibration sections were located within the front section of the cable, previous to, or left of, the damaged area (Figure 3.5). The cable was calibrated for a 10 minute averaging period. Water bath temperatures stayed within ± 0.03°C during

the calibration as monitored using VWR Traceable Digital Thermometers with an accuracy rating of ± 0.001°C.

The calibration trace was later processed using the Agilent recommended method of reducing the calibration trace signal back to the component Anti-stokes and Stokes return signals and recalculating the attenuation ratio and offset. The resulting attenuation and offset calculations did not reproduce bath temperatures well and was not used. The two bath method may have been flawed with the baths close in temperature and utilizing cable sections too closely spaced. The value of this step was the know temperature of the baths that later provided know target temperatures when calculating the temperature offset.

For the second step, the cable damage location was identified and separate corrections for cable attenuation were performed on the front and back sections of cable. The new attenuation correction was found using all points in the front section and 140m immediately beyond the damage. The 140 pts beyond the damage have the most consistent attenuation slope and least amount of variability in both terrain conditions and raw temperatures. The raw temperatures were taken from an in situ temperature trace on February 28, 2008 in the Treeline watershed. The trace had several desirable characteristics. On February 28th, conditions in the watershed had been stable for several days with essentially no melt or runoff coming from the watershed as evidenced by the weir at the mouth of the watershed. The section had a narrow temperature variation of 0.91°C making the linear attenuation obvious and predictable. Attenuation corrections of -0.374 and 0.245dB/km for the front and back sections respectively were calculated and applied to remove the slopes (Figure 3.6).

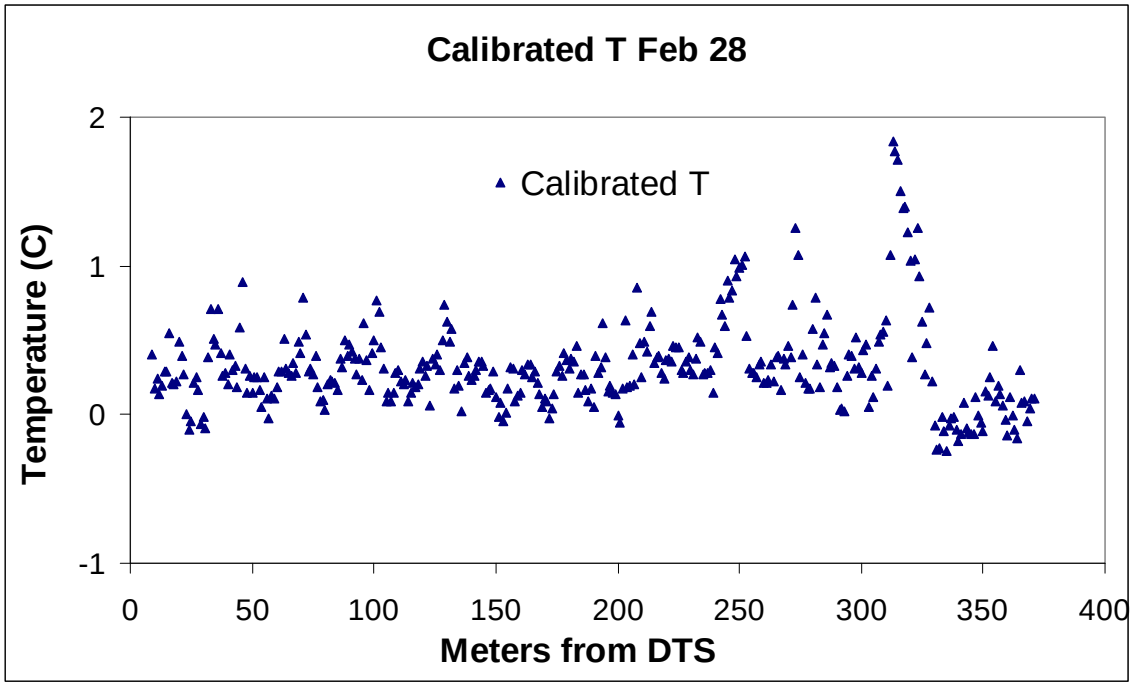

Figure 3.6. Calibrated February trace.

The third step was to find an offset that would match cable temperatures to the bath temperatures from the initial calibration. For this step, the front and back section attenuation corrections were applied to the initial calibration, raw temperature trace from the two bath calibration. Next, the difference was found between the average of the two bath temperatures and average of the two cable sections representing the baths. The difference was added as an offset adjustment to bring the cable temperatures to within 0.01% of each of the respective bath temperatures. Finally, the new offset was applied to the February 28 trace to produce the calibrated plot in Figure 3.6.

3.3.3 Coordination of Cable Location and DTS Point Measurements

Coordinating the DTS point measurements with the corresponding location on the cable is critical to relating near surface soil temperatures to overlying snow depths. Several factors necessitate this coordination. There are meter marks on the buried fiber-

optic cable but they do not coordinate exactly with the distance measured by the machine. The buried cable has been cut arbitrarily and spliced to an intermediate section of connection cable designed to protect the actual connection to the machine. As bare patches of soil emerged in the early melt, it was possible to accurately locate measurement points on the cable. Figure 3.7 shows a temperature trace over two bare soil patches separated by a 1.9m snow patch. Cable meter 1295 has at least ¾ of a meter of soil to each side of it. DTS temperature averaging occurs ½ meter to each side of the point with a rapidly tapering temperature influence for the next ½ meter beyond the theoretical measurement width. Point 1295 represents nearly the true temperature of the soil. Point 1299 is located in a soil patch 1.15m wide. Because the soil temperature is nearly that of the wider soil patch the 1299 cable mark must be nearly centered in the soil patch. From this inference, the DTS point measurements can be coordinated with the numbered cable marks.

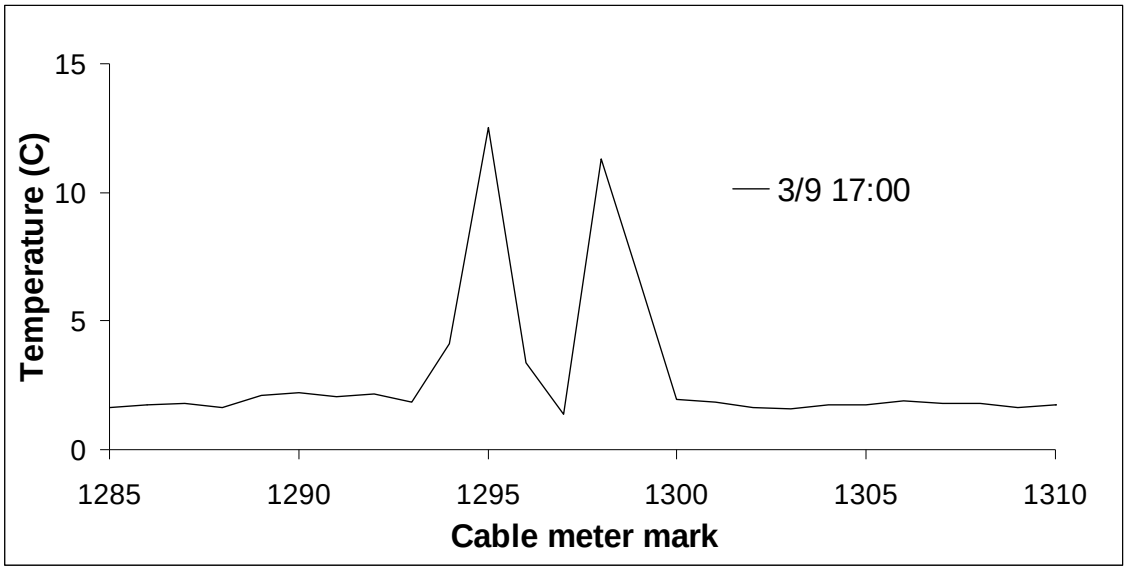

Figure 3.7. Elevated DTS temperature measurements are coincident with narrow bare soil patches allowing coordination of the DTS measurements with precise cable location.

3.4 Ground Heat Flux

3.4.1 Measured Ground Heat Flux

The procedure for calculating ground heat flux (G) from heat flux plates follows the calculations outlined in the Campbell Scientific HFT3 manual (2001). Ground heat flux was measured by averaging two HFT3 ground heat flux plates at 8cm depth. Two pairs of thermocouples over the flux plates at 2 and 6cm depth were averaged to measure the temperature of the overlying soil. A CS615 Water Content Reflectometer at 5cm depth measured the volumetric soil moisture content which is used to adjust the soil conductivity (Cs). The change in soil heat storage (S) is calculated using the following equation:

$$S = \frac{\Delta T_s C_s d}{t} \tag{4}$$

Where ΔT_s is the temperature change during each time interval, d is the depth of measured heat flux (d=0.08m), and t is the time interval. The soil heat flux at the surface (G_{sfc}) is given by:

$$G_{sfc} = G_{8cm} + S \tag{5}$$

3.4.2 Calculating G from DTS Temperature Measurements

The ground heat flux model chosen and modified for this study is based on the equation for one-dimensional steady state heat flow for a homogenous soil media (Equation 3). The assumption of a homogenous media with steady state heat flow remains for the equation but is violated by the actual soil conditions. The varying soil

conditions and implications are discussed in results and discussion section 4.1 "Affects of Soil Temperature Measurement Depth."

The model was chosen primarily for its use of single soil and snow temperatures in establishing a temperature gradient at the snow soil interface and a detailed accounting of vapor diffusion in calculating effective soil conductivity. The original model found in Marks and Dozier (1992) considers the diffusion properties of both the soil and snow and assumes that homogenous, thermally active soil and snow layers are in contact with each other. The thicknesses of the active layers are represented by the distance from the snow soil interface to the temperature measures for the respective layers. In addition, the method applies a vapor diffusion correction to soil and snow conductivities. Ground heat flux is approximated using the following equation from Marks and Dozier (1992):

$$G = \frac{2K_{es}K_{eg}(T_g - T_s)}{K_{eg}z_s + K_{es}z_g} \quad (6)$$

Where K_{es} and K_{eg} are effective snow and soil heat conductivities, T_g and T_s are temperatures of the ground and snow taken at their respective vertical distances from the soil-snow interface Z_g and Z_s.

All of the DTS temperature measurements were made after the commencement of melt when the temperature of the entire snowpack (T_s) was 0°C. Additional energy from the soil cannot raise the temperature of the snowpack and can only cause melt or heating of percolating melt water which is assumed to be immediately removed from the snowpack. Because the snowpack cannot change temperature by storing the additional

energy, conductive properties of the snow are irrelevant and can be removed from equation 6 resulting in the simplified one dimensional equation:

$$G = K_{eg} \frac{(T_g - T_s)}{z_g} \quad (7)$$

The soil thermal conductivity (K_{eg}) is very sensitive to soil moisture. However, the well drained sandy loam soil at Treeline maintained a consistent soil moisture and conductivity throughout the melt period. The thermal conductivity of Treeline sandy loam soil (ρ =1.34 g cm-3, period average θ = 0.18) is 1.13 W m-1 K-1, equal to a value found by (Abu-Hamdeh 2001) for a sandy loam with a density of 1.36 g cm-3 and equal moisture content.

Soil thermal conductivity was corrected for vapor diffusion. Temperature and pressure gradients cause vapor diffusion from warm soil to the snow releasing latent heat of vaporization (Marks and Dozier 1992). In effect, this diffusion changes the thermal conductivity of the soil necessitating an adjustment to create an effective soil conductivity (K_{eg}). The added correction value depends on the assumed saturated specific humidity of the soil (q_g) equal to 4.847 x 10^{-3} (g/kg, dimensionless), and a unique effective water vapor coefficient (D_e). To calculate D_e for local temperatures and pressures, the following equation is applied:

$$D_e = D_{e,o} \frac{P_0}{P_a} \left[\frac{T_s}{T_{melt}} \right]^{n_T} \quad (8)$$

Where $D_{e,o}$ is the effective diffusion coefficient for vapor in saturated soil at sea level (10^{-5} m^{-2} s^{-1}), P_o is sea level pressure (101 kP_a), P_a is the UDCEW pressure (78 kP_a), T_s (273.16 K), and T_{melt} (273.16 K). The exponent, nT (14), is a non-critical value given the temperature relationship and reducing effects of the pressure ratio in the calculation.

The effective conductivity was calculated using the effective diffusion coefficient D_e, specific humidity q_g, and latent heat of vaporization L_v (2.834 x 106 J/kg):

$$K_{es} = K_g + \lfloor L_v D_e q_g \rfloor \quad (9)$$

The correction resulted in a 15% increase to the soil thermal conductivity.

4. RESULTS AND DISCUSSION

The snow year 2007-8 was the sixth largest for 50 years of record (Figure 2.3). The snowpack remained deep into mid-April with shallow areas appearing and melting out quickly due to high air temperatures and sun angles. The south facing slope quickly became patchy presenting the best opportunities to set depth measurement transects over the DTS cable (Figure 4.1). Despite setting several transects, overnight melt outs and a lack of adjacent deep and shallow snow areas over the cable limited the useable transects and data. However, two transects transitioned from deep to bare soil, with mid-day shallow snow, providing enough width for the DTS to resolve soil temperature differences beneath shallow and deep snow (Figure 4.2). Measurement of these transects occurred on 4/11 14:00 and 4/12 17:00. From 4/11 to 4/13, the weather was clear with a 10° C rise in temperature with equal solar input on all three days marking the final meltout of Treeline's southwest facing slope.

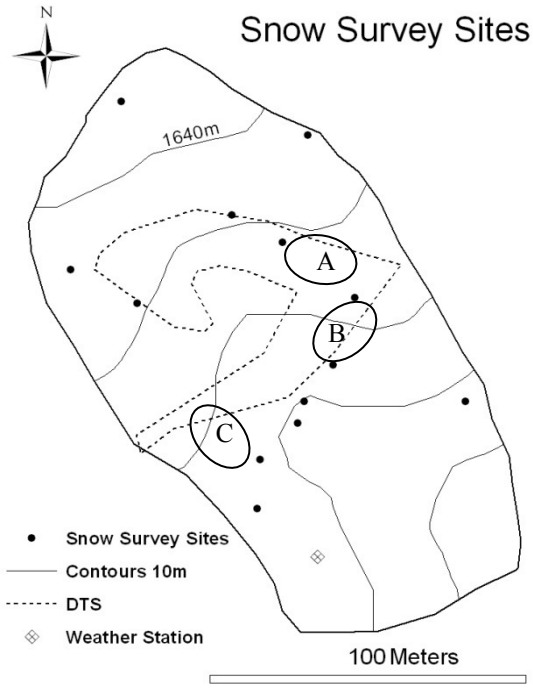

Figure 4.1. Circles represent transect locations above the DTS cable. A is the transect covering meters 1332-1352. B is the transect covering 1375-1406. C is the north facing area where the cable temperatures are compared to soil pit temperature measures.

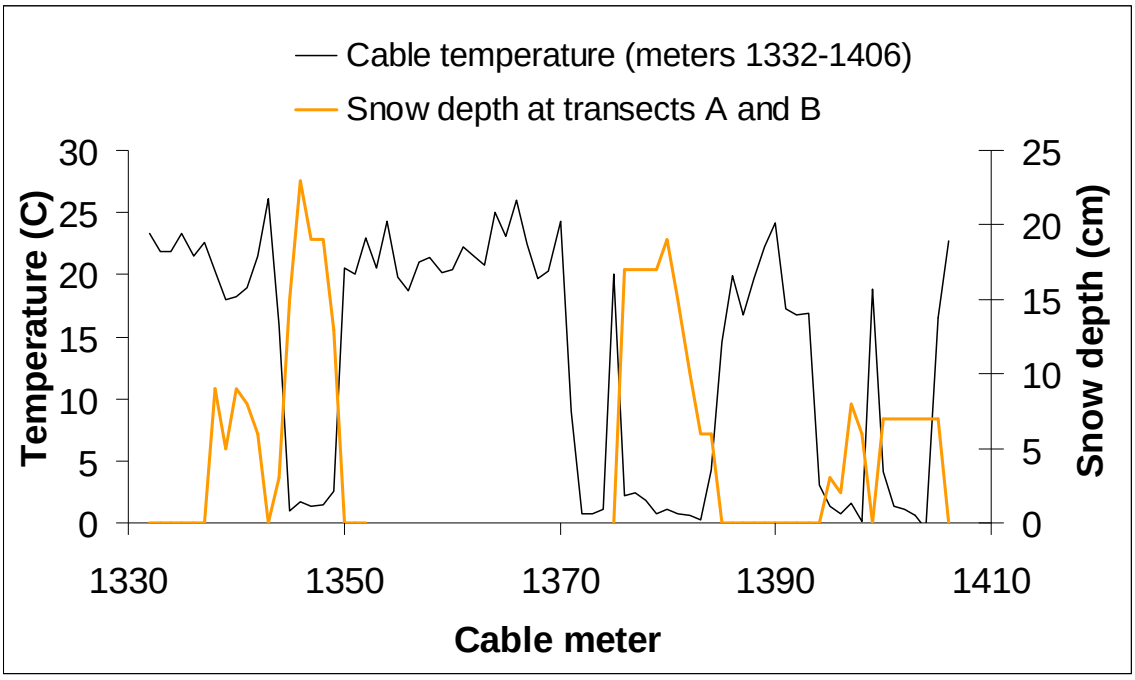

Figure 4.2. Example of DTS cable temperatures resolving overlying snow conditions

4.1 Affects of Soil Temperature Measurement Depth

Soil temperature measurement depth will affect the calculation of ground heat flux because the temperature gradient in the soil column varies with soil depth. The calculation of ground heat flux using Equation 7 treats the soil column as a single layer from the soil-snow interface to the depth of soil temperature measurement (z). Using the single layer, it is assumed that heat transfer is uniform at all depths within the layer.

Heat transfer occurs due to a difference in temperature between media. In a soil column with a uniform linear heat gradient, the rate of heat transfer, or ground heat flux, would be the same at all depths. In this study, the heat gradient is curvilinear with the transfer rate increasing as you approach the soil surface (Figure 4.3). The steepest heat gradient is found in the 0-5cm interval in Figure 4.3. The maximum heat gradient is found at the interface between the soil and 0°C snow.

In summary, using a deeper soil temperature measurement will yield a lower heat transfer expressed as a lower ground heat flux to the snow. To accurately represent ground heat flux, the soil temperature measurement depth must be as close to the soil-snow interface as possible.

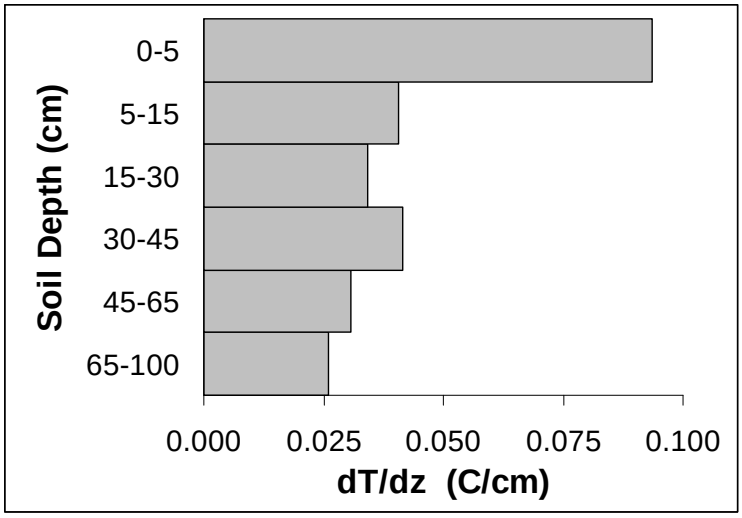

Figure 4.3. Heat gradients (dT/dz) at depth intervals taken on 4/11 14:00 show a curvilinear relationship between soil depth and heat gradient with greater heat transfer near the surface. Soil temperatures are from thermocouples installed in a soil pit at depths 5, 15, 30, 45, 65, and 100cm depth. The 0 depth temperature is that of a melting snowpack, 0°C.

The phenomenon of varying temperature gradients at different depths is further demonstrated with time-series plots in Figure 4.4A-C. The depth of soil between the soil temperature measurement and the overlying snow (0°C) has a great affect on the calculated magnitude of G due to the attenuation of this gradient with greater soil temperature measurement depth. Figures 4.4a-c use atmospheric data from the weather station, soil temperature and moisture data from soil pits at 5 and 45 cm depth, soil temperatures from the DTS at 1.4cm depth, and ground heat flux calculations using Equation 7. The soil temperatures and G from 5 and 45 cm depth can be compared directly. DTS temperatures and G show the capability of the DTS in capturing the weather events and should not be compared directly with soil pit data.

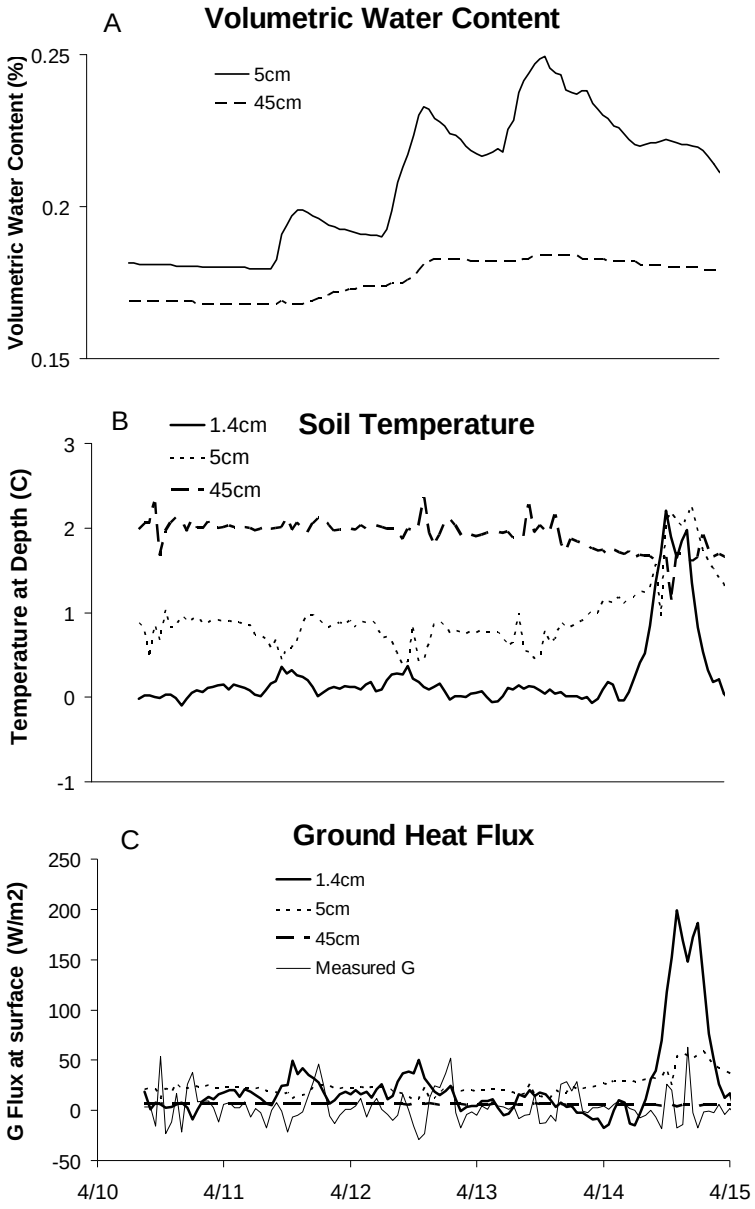

Figure 4.4a-c. Measurement 1.4 is from the DTS, 5 and 45 are from soil pits, and measured G is from heat flux plates. Figure 4.4a shows increasing meltwater influx to the soil on 4/14 to 4/14. On 4/14 a cold front reduces the meltwater influx to the soil surface. Dispersion mutes the soil moisture response at the deeper (45cm) depth. Figure 4.4b shows the rapid melt suppressing soil temperatures at shallow 1.4 and 5cm depths and a delayed suppression at 45cm depth. As infiltration subsides due to a cold front on the 14th, shallow soil temperatures are restored by ground heat flux. Figure 4.4c shows rising near surface temperatures result in increasing G. At 45cm depth, moderated fluctuations in soil moisture and temperature result in a moderated G.

On April 10th through April 14th, the snowpack was reduced from 18 to 15cm depth as clear skies and warm temperatures produced substantial melt infiltration. Near surface soils were flushed with cool melt water while the soil at 45 cm remained warm due to a delay in the wetting front from the cold melt (Figure 4.4b). As a cold front moved in on the 14th, surface melt and the cold flushing of surface soils tapers off as the snowpack drains its remaining meltwater and soil volumetric water content declines (Figure 4.4a). The near surface soil temperature was then restored by ground heat from below (Figure 4.4B). The moderating affects of the deeper soil have masked the near surface fluctuations in modeled G and violated the assumptions of the heat transfer equation. As the near surface soil temperatures rise, and without the buffering capacity of a thick soil layer, G increases substantially along the increased soil-snow temperature gradient.

In summary, the model does not account for the variations in heat gradient with soil depth. If heat were being transferred to the snow pack, as you would find with snowpacks below 0°C, the near surface soil temperature measurement is better than the deeper because the near surface soil better reflects temperature gradients near the snow soil interface. In the case of ripe melting snowpacks, any ground heat flux reaching the snowpack will result in more melt with no change in temperature of the snow. During this study, melt rates of up to 4cm SWE per day have likely eliminated the heat gradient between the soil and snow, essentially eliminating ground heat flux to the snow. Under these conditions, the ground heat flux that remains will heat the influx of melt.

There is another source of ground heat flux worth noting. In addition to ground heat, patchy snow receives lateral heat transfer from adjacent bare soil to soil beneath the snow margin. On April 18th 9:00-10:00, pairs of ground heat flux plates were placed

vertically in the soil: one at the snow margin and the other 10 cm away from the snow margin. Positive readings indicate heat fluxes toward the snow with negative fluxes away from the snow. Of the 16 measurements taken, the average flux for the plates 10cm from the snow margin was 6W/m^2 with both positive and negative values. The average of the plates at the snow margin was 49W/m^2 with all positive values. This flux is capable of warming the soil under the snow margin and accelerating melt.

4.2 Measured Soil Temperature and Calculated Ground Heat Flux

Two transects were used in this analysis of soil temperature and G flux beneath shallow and deep snow. The first transect data taken on 4/11/08 14:00 included 21 meters of cable from 1332-1352 (Figure 4.1 transect A), the second section on 4/12/08 17:00 included 32 meters from 1375-1406 (Figure 4.1 transect B). Two transect locations were chosen in this analysis because each had comparable adjacent patches of shallow snow, deep snow, and bare soil of sufficient width for the DTS to resolve the temperature and ground heat flux values without direct influences to the cable from the adjacent, dissimilar snow conditions. The two transects used in this study were located on a similar aspect with common antecedent soil moisture conditions from previous melt rates of 2-4cm SWE per day. However, there are notable differences between the two transect locations. The 4/11 transect had no brush, ran perpendicular to the more moderate slope, was closer to the snow free ridge top, and was measured at 14:00. The 4/12 transect had sage brush near the cable, the cable ran down the fall line of a steeper slope, was farther down slope with snow above the transect, and was measured at 17:00, a time with half the incoming solar of the previous day. Table 4.1 summarizes the meteorological conditions at the time of measurement for the two days. The snow depths are averages for point measurements under a given snow condition. Each point used under a given snow condition is at least one meter from adjacent conditions. The soil depth averages are the burial depth for the section of cable beneath the given snow condition. Figure 4.5 shows the twenty-four hour range of soil temperatures for 4/11 and 4/12 under the three snow conditions of interest.

Table 4.1. Meteorological, snow, and DTS burial conditions for two transects.

Parameter	4/11/08 14:00	4/12/08 17:00
Air temperature (ºC)	5.7	13.0
Precipitation rate (m/h)	0.0	0.0
Wind speed (m/s)	2.0	0.9
Relative humidity (%)	0.53	0.44
Incoming solar (W/m^2)	846	468
Net solar (W/m^2)	877	486
Soil depth to cable for shallow snow (cm)	1.2	1.7
Soil depth to cable for deep snow (cm)	1.2	2.0
Snow depth shallow (cm)	7	6
Snow depth deep (cm)	18	17
T of soil for shallow snow (°C)	1.5	0.8
T of soil for deep snow (°C)	0.9	1.3
G under shallow snow (W/m^2)	215	49
G under deep snow (W/m^2)	100	96

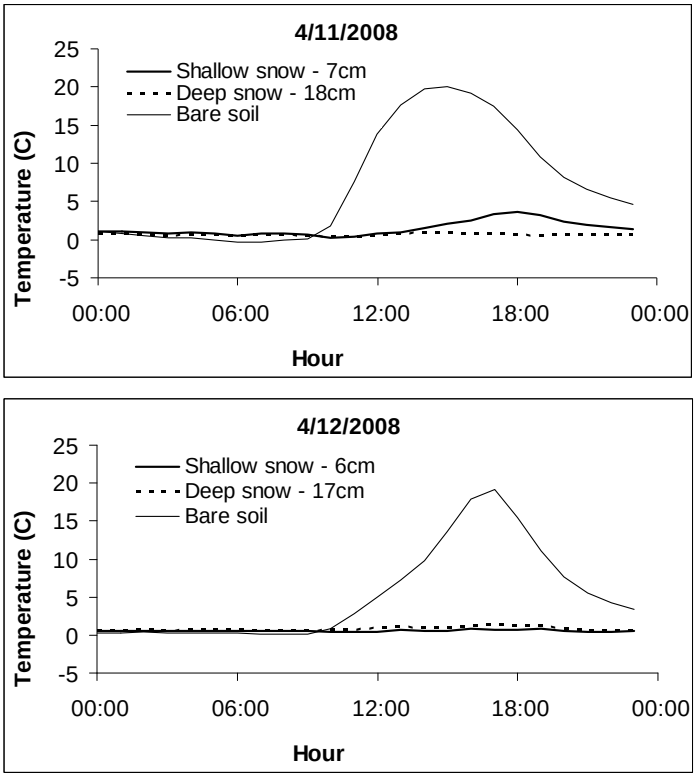

Figure 4.5. Soil temperature ranges for 24 hour periods on 4/11 and 4/12. The soil temperature averages are for all readings below the stated snow condition and associated average snow depth.

Soil temperatures were similar for both transect locations on both days. On 4/11, soil temperatures beneath shallow and deep snow were 1.5 and 0.9°C with bare soil temperatures averaging 19.7°C (Figure 4.6-4/11). On 4/12, soil temperatures beneath shallow and deep snow were 0.8 and 1.3°C with bare soil averaging 19.2°C (Figure 4.6-4/12). Figure 4.6 shows corresponding G values calculated from soil temperatures for each day respectively. For 4/11, shallow snow G was 215W/m^2 and for deep snow, 100W/m^2 (Figure 4.7-4/11). On 4/12, G for shallow snow was 49W/m^2 and for deep snow, 96W/m^2 (Figure 4.6-4/12). The soil temperatures beneath shallow and deep snow account for the difference in modeled G on 4/11 (Figure 4.7-4/11). Differences in 4/12 soil temperature and measurement depth (z_g) account for differences in G beneath shallow and deep snow (Figure 4.7-4/12). The deeper cable depths on 4/12 have moderated the heat flux when compared to 4/11.

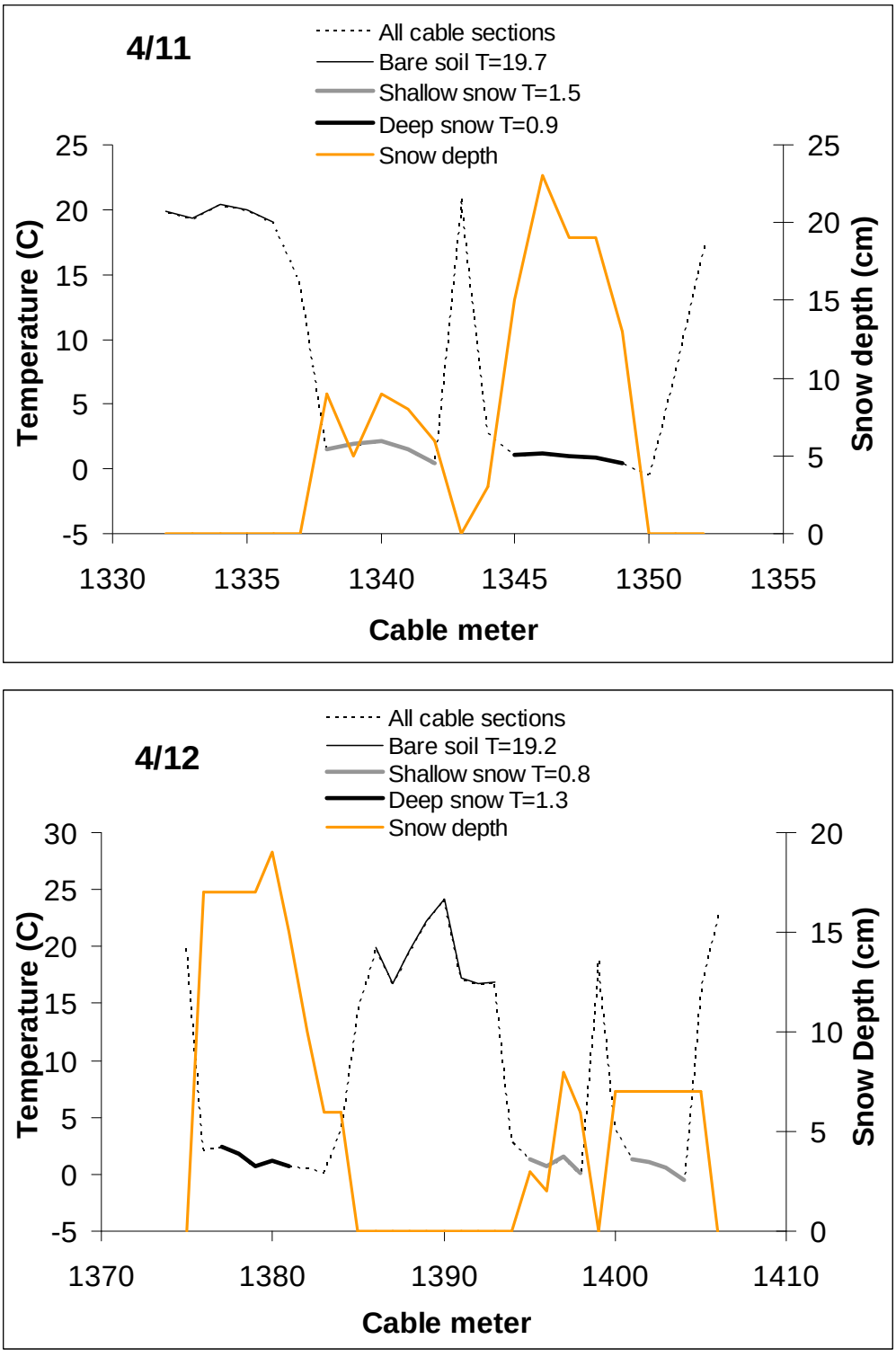

Figure 4.6. Soil temperatures below shallow and deep snow and bare soil for transects on 4/11 14:00 and 4/12 17:00.

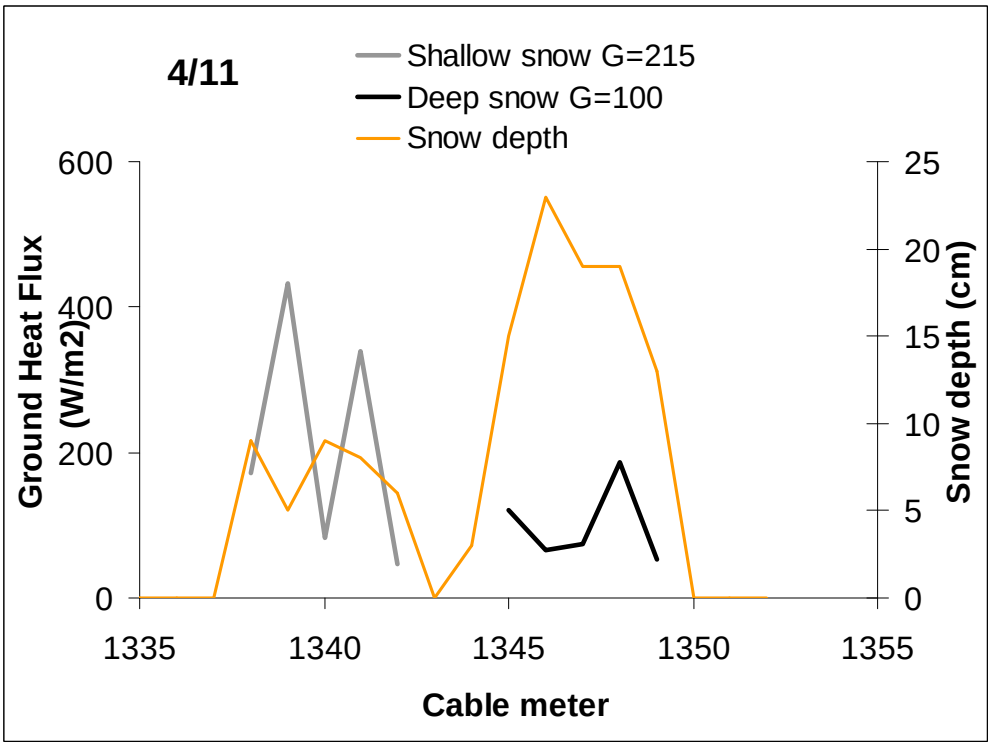

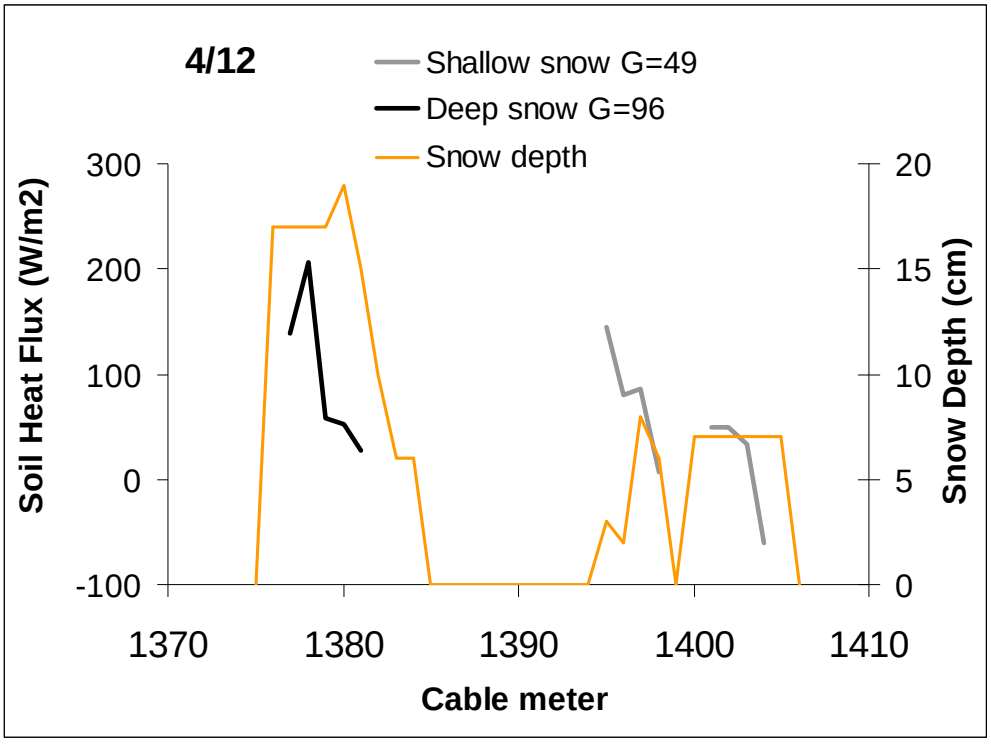

Figure 4.7. Ground heat flux for two transects on two days beneath shallow and deep snow. Differences in heat flux arise from differences in soil temperature and measurement depth.

Elevated April 11th soil temperatures beneath shallow snow when compared to deep snow may be attributable to varying factors. At 14:00 hours the sun is delivering over 800W/m^2 to the shallow snow surface. However, solar penetration reaching the snow soil interface, through 7cm of snow, is less than 5% of the incident radiation according to the solar extinction curve presented in Figure 1.3. The energy gained at the snow/soil interface would result in a small increase in melt and further remove a temperature gradient between the snow and soil. It is unlikely that this would result in a 0.6°C heating of the meltwater and soil volume (1.5°C) above and around the cable when compared to the adjacent soil (0.9°C) below deeper snow.

By the next day, the shallow area of the April 11 transect was snow free. On April 11, the soil temperature rises throughout the afternoon (Figure 4.4). This may indicate that that later in the day the snow has become very shallow, less than 2cm deep, when 70% of the incident solar can reach the snow soil interface (Figure 1.3). Had this section become snow free, a rapid rise in soil temperature should have appeared as a break in slope, independent of the sinuous daytime curve. A more likely scenario is that adjacent bare soil is influencing or encroaching on the transect causing the DTS to average in high temperature, bare soil influences. It should also be noted that there was no snow upslope of this transect. With its perpendicular positioning, there is little to no excess water flushing across the transect from above to moderate the heating of adjacent bare soil.

Soil temperatures were insignificantly elevated for deep snow on April 12 (Figure 4.5) rather than shallow snow as found on April 11. This is likely due to cable averaging and adjacent conditions with brush and bare soil patches causing greater temperature variations under both snow conditions. The significant difference between the two days is

found in the 24 hour plots of soil temperatures for the two transects (Figure 4.5). On 4/12, soil temperatures beneath both shallow and deep snow areas remained similar and suppressed throughout the day. The soil temperatures are also similar to the deep snow area of the 4/11 transect. This indicates that the availability of meltwater from overlying snow is driving the near surface soil temperature regime. The 4/12 transect runs down the fall line of the twenty degree hill slope with patchy snow above the transect and the deeper snow area upslope of the shallow snow area. With melt rates of 2 to 4cm SWE per day, there is a substantial amount of cold water flowing laterally through the soil from above the transect into the deeper snow section, and from the deeper snow section into the soils beneath the shallow snow section. This would also be true for the 4/11 transect until sections became snow free. This large amount of cold melt and lateral flow has suppressed the soil temperatures in both sections of the cable with snow cover.

In summary, the near surface soil temperature is held close to 0°C beneath deep, $\geq$10cm, or shallow snow cover of 6-7cm. Temperatures for bare exposed saturated soils for both transects were equal despite their location on the hill slope indicating that exposure to large magnitude solar radiation can heat the near surface saturated soils quickly even when only few meters down slope from a meltwater source. The progression of soil temperatures beneath the shallow snow on 4/11 is likely due to instrument temperature averaging and a proximal receding snow margin. However, the progression also suggests that very shallow snow, with its porous nature, may allow enough solar energy to penetrate and begin heating the soil in its transition to complete ablation and bare exposure.

4.3 DTS Use Under Snowpacks

Use of the DTS system in snow over extended periods presents many unique problems. The precision of the instrument may not match its accuracy for the intended purpose. Fiber cable must be installed prior to the winter season and may be out of step with the availability of the DTS machine jeopardizing a good calibration. Power is a problem over extended periods. Despite the ruggedness of the DTS, natural conditions can be unpredictable and costly.

The averaging scheme of the DTS is an important consideration in capturing accurate and precise measurements. The DTS is capable of measuring temperatures to 0.04°C but does so by averaging over a distance. With this property, adjacent conditions may reduce accuracy of the measurement. In the case of this study, lateral snow melt caused the shallow edges of snow margins to recede so quickly that it was difficult to find patches of shallow snow of sufficient width to produce an accurate temperature without the influence of the actively encroaching bare soil conditions.

With snow studies, it is common to measure undisturbed conditions necessitating an early installation of the fiber cable. Due to high instrument costs and increasing demands for borrowed DTS equipment, logging time may be limited or out of step with other elements of your study. In this case, the period of interest was throughout the spring melt, months after the cable installation. The calibration was done on the cable after extricating it from the study site. The fragile connectors on the ends of the cable are prone to breakage and deterioration of signal transmission with every insertion or withdrawal from junction points. This can create problems with calibrations done on a cable and connecters that have spent time under snow, soil, or water. In the case of this

study, deteriorating connectors rendered calibration efforts useless. To remedy the problem, a new connector was spliced to the cable and a calibration performed. Using a different connector for the calibration of the cable may affect the processing of all of the previous data.

One of the great advantages of the DTS is the temporal resolution. The DTS can be programmed to match the sampling interval of other instruments in a study. However, this requires an adequate power supply for continuous measurement. In this study, a sufficient size solar panel (195 Watt) to power the DTS in the winter months was too costly. The solution was a bank of batteries and a gas powered generator. My site required three large RV batteries to power the DTS and a laptop for 1½ days between charges. The demands of this power system precipitated gaps in the data. Although the battery solution cuts costs and is reasonable for a few days, the difficulty in transporting the batteries and maintaining the charge should be carefully considered especially with remote locations.

Finally, natural conditions are hard on the fiber cable. The DTS machine held up extremely well for the two months it spent in winter conditions. However, the fiber-optic cable is prone to damage. The connectors are very fragile and must be protected at all times. The cable, despite the multiple all-terrain coatings, can easily be severed by rodents. The UDCEW is in a migratory corridor for Elk herds. One morning I found several Elk had walked on and pushed my cable farther into the soil for a distance of 30 meters. Be careful with the cable and, if possible, calibrate and test it for damage using the DTS before it is deployed in the field.

The DTS is a unique and versatile tool yielding high temperature, temporal, and spatial resolutions. Using the DTS should be carefully considered with respect to spatial scale, availability of equipment, maintenance while in use, and the likely hood of damage over long periods of use.

5. CONCLUSIONS

The goal of this study was to accurately measure ground heat flux and assess the contribution of ground heat flux to the energy balance of shallow snow less than 10cm depth. Because instruments for measuring G must be placed in the ground prior to snow accumulation and before the locations of shallow and patchy snow are known, a method for obtaining snow-soil interface temperatures at high spatial and temporal resolutions is required. DTS offers a solution with limitations imposed by a spatial averaging scheme that may bring adjacent conditions into point temperature measurements. Regardless, the precision of distributed relative temperature measurements with the DTS coupled with absolute G measurements at limited locations provide insight into the dynamics of G in shallow, patchy snow and offers considerations for future use of DTS in snow applications.

Ground heat flux beneath shallow patchy snow must be modeled from soil temperatures due the need for high spatial measurements currently available only for temperature. The models are based on the assumption of steady state heat flux throughout the soil column. In this study soil temperatures showed a cooling trend from 100cm depth to the soil surface with temperature gradients the highest between 5cm soil depth and the snow. This violation of steady state has strong implications when considering soil temperature measurement depth and the calculation of ground heat flux. For the non-uniform temperature soil column found in this study, calculated magnitude of

G was inversely related to soil temperature measurement depth, a situation not accounted for in the heat transfer equation assumptions.

Light energy can penetrate snow to the soil surface but follows an exponential extinction curve as snow depth increases. As an example, 70% of incident light can reach the soil surface through 2cm snow depth but is almost eliminated through 10cm of snow. In this study of late season shallow snowmelt, two transects measuring soil temperatures were used in calculating and comparing ground heat flux beneath two overlying snow conditions: shallow snow 6-7 cm depth and snow >10cm depth. A transect taken on 4/11 14:00 showed a 0.6°C higher soil temperature below shallow snow when compared to the deep snow. This higher temperature also results in a greater calculated ground heat flux for shallow snow. Under 6-7 cm of snow, light penetration is <5% which cannot transfer enough energy to the soil surface to cause a 0.6°C warming of the saturated soil above and around the DTS cable. A proximal and approaching snow margin may have allowed the higher temperature bare soil to conduct heat to the soil under the shallow snow and influence the temperature measurement. However, the shallow snow was gone by the following day indicating that the shallow area may have progressed through a very shallow depth <2cm during the late afternoon following the 14:00 depth measurements. This progression may have allowed enough solar penetration and associated energy flux to be partially responsible for the increasing soil temperatures under the shallow snow as the day progressed.

Using the DTS deserves careful consideration with respect to spatial scale, availability of equipment, maintenance while in use, and the likely hood of damage over long periods of use. Some difficulties are exacerbated in snow studies due to early cable

placement, previous to the snow season, prior to calibration. The sustained exposure to natural elements and use can adversely affect the cable connectors and expose the fiber-optic cable to damage due to handling in rough terrain or damage from wildlife. This damage can result in a compromised calibration which in turn may compromise the collected data. Despite the complications of shallow snow, the DTS is a unique and versatile tool yielding high temperature, temporal, and spatial resolutions and its explored in other snow applications.

REFERENCES

Abu-Hamdeh, N. H. (2001). "Measurement of the Thermal Conductivity of Sandy Loam and Clay Loam Soils using Single and Dual Probes." J. agric. Engng Res. 80(2): 209-216.

Baker, D. G., Skaggs, R. H., and Ruschy, D. L. (1991). "Snow Depth Required to Mask the Underlying Surface." Journal of Applied Meteorology 30(3): 387-392.

Bales, R. C., Molotch, N. P., Painter, T. H., Dettinger, M. D., Rice, R., and Dozier, J. (2006). "Mountain hydrology of the western United States." Water Resour. Res. 42(8): 13.

Barnett, T. P., Adam, J. C., and Lettenmaier, D. P. (2005). "Potential impacts of a warming climate on water availability in snow-dominated regions." Nature 438: 303- 309.

Blöschl, G. and Kirnbauer, R. (1992). "An analysis of snow cover patterns in a small alpine catchment." Hydrological Processes 6(1): 99-109.

Campbell, S. I. (2003). Instruction manual for the HFT3 soil heat flux plate**:** 12 pp.

Cayan, D. R., Kammerdiener, S. A., Dettinger, M. D., Caprio, J. M., and Peterson, D. H. (2001). "Changes in the onset of spring in the western United States." Bull. Am. Meteorol. Soc. 82((3)): 399- 415.

Chung, Y. C. and England, A. W. (2006). The Influence of Snow–Soil Moisture Flux on Snowpack Metamorphism in Late Winter and Early Spring. 63rd Eastern Snow Conference. Newark, Delaware USA.

Cline, D. W. (1997). "Snow surface energy exchanges and snowmelt at a continental, midlatitude Alpine site." Water Resources Research 33(4): 689-701.

Dingman, S. L. (2002). Physical Hydrology. New Jersey, Prentice Hall, Inc.

Dorighi, J. (2009a). DTS Averaging Scheme. Personal communication: February 13.

Dorighi, J. (2009b). Two section calibration for damage. Personal communication: April 10.

Dozier, J. and Painter, T. H. (2004). "Multispectral and hyperspectral remote sensing of alpine snow properties " Annu. Rev. Earth Planet. Sci. 32: 465–94.

Essery, R., Granger, R., and Pomeroy, J. (2006). "Boundary-layer growth and advection of heat over snow and soil patches: modeling and parameterization." Hydrological Processes 20(4): 953-967.

Flerchinger, G. N. and Saxton, K. E. (1989). "Simultaneous heat and water model of a freezing snow-residue-soil system: I. Theory and development." Trans. ASAE 32: 573-578.

Garen, D. C. and Marks, D. (2005). "Spatially distributed energy balance snowmelt modeling in a mountainous river basin: estimation of meteorological inputs and verification of model results." Journal of Hydrology 315(1-4): 126-153.

Granger, R. J., Essery, R., and Pomeroy, J. W. (2006). "Boundary-Layer Growth Over Snow and Soil Patches: Field Observations." Hydrological Processes 20: 943-951.

Grey, D. M. and Male, D. H. (1981). Handbook of Snow: Principles, Processes, Management and Use. Toronto, Pergamon Press.

Gribb, M. M., Forkutsa, I., Hansen, A., Chandler, D. G., and McNamara, J. P. (2009). "The Effect of Various Soil Hydraulic Property Estimates on Soil Moisture Simulations." Vadose Zone Journal 8: 1-12.

Hawkins, T. W. and Ellis, A. W. (2007). "A Case Study of the Energy Budget of a Snowpack in the Arid, Subtropical Climate of the Southwestern United States." Journal of the Arizona-Nevada Academy of Science 39(1): 1-13.

Jordon, R. (1991). "A one-dimensional temperature model for a snow cover: Technical documentation for SNTHERM.89." Spec. Rep. 91-16, U.S. Army Corps of Eng., Cold Reg. Res. and Eng. Lab., Hanover, N.H.

Liston, G., E. (1995). "Local Advection of Momentum, Heat, and Moisture during the Melt of Patchy Snow Covers." J. Appl. Meteor. 34: 1705-1715.

Luce, C. H. and Tarboton, D. G. (2001). Modeling snowmelt over an area: Modeling subgrid scale heterogeneity in distributed model elements. MODSIM 2001, International Congress on Modeling and Simulation. Canberra, Australia, Modell. and Simul. Soc. of Aust. and N. Z. Inc.

Marks, D. and Dozier, J. (1992). "Climate and Energy Exchange at the Snow Surface in the Alpine Region of the Sierra Nevada 2. Snow Cover Energy Balance." Water Resources Research 28(11): 3043-3054.

Marks, D. and Winstral, A. (2001). "Comparison of Snow Deposition, the Snow Cover Energy Balance, and Snowmelt at Two Sites in a Semiarid Mountain Basin." Journal of Hydrometeorology 2(3): 213-227.

Marsh, P. (1999). "Snowcover formation and melt: recent advances and future prospects." Hydrological Processes 13(14-15): 2117-2134.

Mazurkiewicz, A. B., Callery, D. G., and McDonnell, J. J. (2008). "Assessing the controls of the snow energy balance and water available for runoff in a rain-on-snow environment." Journal of Hydrology 354: 1-14.

McNamara, J. P., Chandler, D., Seyfried, M., and Achet, S. (2005). "Soil moisture states, lateral flow, and streamflow generation in a semi-arid, snowmelt-driven catchment." Hydrological Processes 19(20): 4023-4038.

Mote, P. W., Hamlet, M. P., and Lettenmaier, D. P. (2005). "Declining mountain snowpack in western North America." Bull. Am. Meteorol. Soc. 86((1)): 39-49.

Nayak, A. (2008). Wind Correction program. Logan, Utah, Utah State University

Neumann, N. and Marsh, P. (1998). "Local advection of sensible heat in the snowmelt landscape of Arctic tundra." Hydrological Processes 12(10-11): 1547-1560.

NOAA (2001). Climatography of the United States No. 20 1971-2000, National Oceanic & Atmospheric Administration.

NRCS (2008). Snow course historical data, Natural Resource Conservation Service-USDA National Water and Climate Center's ftp anonymous server.

O'Neill, A. D. J. and Gray, D. M. (1973). Solar radiation penetration through snow. Proc. of UNESCO-WMO-IAHS Symposia on the Role of Snow and Ice in Hydrology, IAHS Press, Wallingford, UK. .

Olyphant, G. A. and Isard, S. A. (1988). "The Role of Advection in the Energy Balance of Late-Lying Snowfields: Niwot Ridge, Front Range, Colorado." Water Resources Research 24(11): 1962-1968.

Pomeroy, J. W., Toth, B., Granger, R. J., Hedstrom, N. R., and Essery, R. L. H. (2003). "Variation in Surface Energetics during Snowmelt in a Subarctic Mountain Catchment." Journal of Hydrometeorology 4(4): 702-719.

Selker, J. S., L. Thévenaz, H. Huwald, A. M., W. Luxemburg, N. van de Giesen, M. Stejskal, J. Zeman, M. Westhoff, and Parlange, M. B. (2006). "Distributed fiber-optic temperature sensing for hydrologic systems." Water Resour. Res. 42.

Sensoy, A., Sorman, A. A., Tekeli, A. E., Sorman, A. U., and Garen, D. C. (2006). "Point-scale energy and mass balance snowpack simulations in the upper Karasu basin, Turkey." Hydrol. Process. 20: 899–922.

Smith, R., Moore, R., and Weiler, M. (2007). Midwinter Snowmelt Generated by Ground Heat Flux: Implications to Catchment Hydrology. AGU San Francisco.

Smolen, J. J. and van der Spek, A. (2003, April 18, 2009). "Distributed Temperature Sensing: A DTS Primer for Oil & Gas Production." Retrieved April 18, 2009,

from http://www.witsml.org/images/witsml/schemas/1311/doc/Shell_DTS_Primer.pdf.

Soto, M. A., Sahu, P. K., Faralli, S., Sacchi, G., Bolognini, G., Pasquale, F. D., Nebendahld, B., and Rueck, C. (2007). High performance and highly reliable Raman-based distributed temperature sensors based on correlation-coded OTDR and multimode graded-index fibers. Third European Workshop on Optical Fibre Sensors, SPIE.

Stewart, I. T., Cayan, R. D., and Dettinger, M. D. (2005). "Changes toward earlier streamflow timing across western North America." Journal of Climate 18: 1136-1155.

Tyler, S. W., Burak, S. A., McNamara, J. P., LaMontagne, A., Dozier, J., and Selker, J. (2008). "Spatially Distributed Temperatures at the Base of Two Mountain Snowpacks Measured with Fiber Optic Sensors."

Williams, C. J. (2005). Characterization of the spatial and temporal controls on soil moisture and streamflow generation in a semi-arid headwater catchment. Department of Geosciences. Boise, Idaho, United States, Boise State University. M.S.

Yang, D., Goodison, B. E., Metcalfe, J. R., Golubev, V. S., Bates, R., Pangburn, T., and Hanson, C. L. (1998). "Accuracy of NWS 80 Standard Nonrecording Precipitation Gauge: Results and Application of WMO Intercomparison." Journal of Atmospheric and Oceanic Technology 15: 54-68.

Yenko, M. K. (2003). Hydrometric and geochemical evidence of streamflow sources in the Upper Dry Creek Experimental Watershed, Southwestern Idaho. Geology. Boise, Idaho, Boise State University. Masters of Science in Geology**:** 128.

Zuzel, J. F. and Cow, L. M. (1978). Ablation of an Isolated Snowdrift. Modeling of Snow Cover Runoff, Hanover, N.H., U.S. Army cold Regions Research and Engineering Laboratory.

Zuzel, J. F. and Cox, L. M. (1975). "Relative Importance of Meteorological Variables in Snowmelt." Water Resourses Research 11(1): 174-176.